TOPICAL REVIEW • OPEN ACCESS

Phase transition of 2D van der Waals ferroelectrics

To cite this article: Wei Han *et al* 2025 *2D Mater.* **12** 032002

2D Materials

TOPICAL REVIEW

Phase transition of 2D van der Waals ferroelectrics

Wei Han[1,2,6,8], Jiayun Wei[6,8], Hao Wang[2,6,*], Shu Ping Lau[1,*], Thuc Hue Ly[3,4,5,*] and Jiong Zhao[1,7,*]

[1] Department of Applied Physics, The Hong Kong Polytechnic University, Kowloon, Hong Kong, People's Republic of China
[2] Hubei Yangtze Memory Laboratories, Wuhan 430205, People's Republic of China
[3] Department of Chemistry and Center of Super-Diamond & Advanced Films (COSDAF), City University of Hong Kong, Kowloon, Hong Kong, People's Republic of China
[4] Department of Chemistry and State Key Laboratory of Marine Pollution, City University of Hong Kong, Hong Kong Special Administrative Region of China, People's Republic of China
[5] City University of Hong Kong Shenzhen Research Institute, Shenzhen, People's Republic of China
[6] Institute of Microelectronics and Integrated Circuits, School of Microelectronics, Hubei University, Wuhan 430062, People's Republic of China
[7] The Hong Kong Polytechnic University Shenzhen Research Institute, Shenzhen, People's Republic of China
[8] These authors contribute equally to this work.
[*] Authors to whom any correspondence should be addressed.

E-mail: wangh@hubu.edu.cn, apsplau@polyu.edu.hk, thuchly@cityu.edu.hk and jiongzhao@polyu.edu.hk

Keywords: phase transition, van der Waals ferroelectric, 2D material

Supplementary material for this article is available online

OPEN ACCESS

RECEIVED
26 November 2024

REVISED
28 March 2025

ACCEPTED FOR PUBLICATION
12 May 2025

PUBLISHED
27 May 2025

Abstract

Two-dimensional (2D) van der Waals ferroelectrics with switchable electric polarization offer exciting possibilities in the fields of physics, materials science, and device engineering. Beyond the conventional polarization-state regulation through electric-field, 2D ferroelectrics can offer important additional functionalities through isomeric phases, including paraelectric and antiferroelectric phases. In recent years, a variety of novel ferroelectric orders have been discovered in 2D materials, resulting from intra- or inter-layer symmetry-breaking. These hidden phases, exhibit attractive properties, and understanding their phase transition mechanisms and controlling the transitions has become a central topic in the field of 2D ferroelectrics. Furthermore, phase control is a primary step towards scalable synthesis of 2D ferroelectrics and device applications. Here, we highlight the diverse mechanisms of the phase transitions in 2D ferroelectrics, particularly intrinsic and extrinsic ferroelectrics. We also summarize different approaches and respective conditions for phase control. Moreover, the *in situ* experimental techniques for studying phase transitions, and the rationalized scalable synthetic methods of 2D ferroelectrics are discussed. Finally, rich functionalities, opportunities and emerging applications combining phase control and ferroelectricity in phase-change ferroelectric devices are envisioned, with the remaining challenges briefly discussed.

1. Introduction

Ferroelectrics are featured with spontaneous electric polarization that can be reversed by an electric field. Since the discovery of the first ferroelectric compound Rochelle salt in 1921, ferroelectrics have been studied in several fields, including physics, chemistry, materials science and engineering applications, for over a century [1]. Many traditional perovskite ferroelectrics, such as $BaTiO_3$, [2] $BiFeO_3$, [3] and $PbTiO_3$, [4], which have been reported, are insulating with wide bandgaps (2.5–3.5 eV) and three-dimensional (3D) lattices, which limit their potential applications in devices. The emergent two-dimensional (2D) materials, [5] such as graphene and transition-metal dichalcogenides (TMDs), [6] possess tunable bandgap range (0–2.5 eV), atomic thickness, absence of dangling bonds, flexibility, and quantum confinement effects. These materials have caused a great research upsurge and are highly viable for a wide range of potential applications [7]. As the exploration of novel physical properties and the need for device miniaturization, the field of van der Waals (vdW) ferroelectric materials is rapidly growing. 2D vdW ferroelectrics can be classified into two categories: intrinsic ferroelectrics, [8, 9] such

Table 1. Comparison of traditional ferroelectrics and 2D vdW ferroelectrics.

Item	Traditional ferroelectrics	2D vdW ferroelectrics	References
Structure	Non-layered; with dangling-bond; strong covalent or ionic bond; without vdW gap	Layered; atomic thin; without dangling-bond; weak interlayer vdW bond; strong intralayer covalent bond; possessing vdW gaps	[19]
Origin of ferroelectricity	Ionic-displacement; polar molecular groups; spin-driven polarization	Ionic-displacement; charge-redistribution; spin-driven polarization	[2, 20, 21]
Ferroelectric properties	Large polarization intensity of 10–100 μCcm^{-2}	Small polarization intensity of 3.5 μCcm^{-2} ($CuInP_2S_6$)	[22, 23]
Stability	Most are stable under ambient conditions	Many are unstable under ambient conditions	[23]

as SnTe, [10] and extrinsic ferroelectrics, [11] such as homo- or hetero-stacked bilayer structures [12, 13]. Furthermore, 2D vdW ferroelectrics hold great potential for a wide range of applications, including beyond-Boltzmann transistors [14, 15], ferroelectric field-effect transistors [16], in-memory sensors [17], and neuromorphic computing [18].

The transition from 3D to 2D vdW ferroelectrics introduces a myriad of remarkable properties due to the reduced lattice dimensionality. These include layer-number-dependent polarization, quadruple-well ferroelectricity, metallic ferroelectricity, moiré ferroelectricity, twisted ferroelectricity, interfacial ferroelectricity, sliding ferroelectricity, and stacking ferroelectricity, etc. [10]. We give a comparison of traditional ferroelectrics and 2D vdW ferroelectrics, as listed in table 1, regarding structure, [19] origin of ferroelectricity, [2, 20] dimension dependence, [21] substrate dependence, [22] and ferroelectric properties [23]. Despite significant differences in structure and dimension, traditional ferroelectrics and 2D vdW ferroelectrics share certain similarities and connections in terms of the origin of ferroelectricity.

Ferroelectrics normally undergo intrinsic ferroelectric phase transition at Curie temperature (T_c) [24]. Ferroelectricity exists only below T_c, while the spontaneous electric polarization vanishes above T_c and leads to the paraelectric phase. Previously, the ferroelectrics community mostly focused on elevating T_c to ensure a large temperature window and sufficient stability for ferroelectric phases [25]. In other words, the paraelectric or other phases have been overlooked. Therefore, most ferroelectric devices only exploit the reversible polarization dipoles in the ferroelectric phases [26]. Phase transitions, including ferroelectric phase transitions, can be induced by various means beyond temperature, such as mechanical strain, electric field/charge doping, stacking order, thickness, etc. [27–30]. The large surface-to-volume ratio, vdW layered structure, and ultrahigh flexibility make 2D ferroelectrics easier to undergo breaking of symmetry and phase transitions [31]. This means that, in addition to the conventional modulation of electric polarization, 2D ferroelectrics have more degrees of freedom brought by the extra phases or so-called polymorphs [32]. For instance, there are abundant phases in 2D $MoTe_2$, including 3 R, 2 H, 1 T, 1 T′, and T_d, but only T_d phase is proved to be the intrinsic ferroelectric [33, 34]. 2D In_2Se_3 is also notable for its polymorphism. The energy difference among its α, β, and β' phases is not significant, making it easy for them to transform into each other [35]. Similarly, MX compounds (where M = In, Ga, Ge and X = S, Se, Te) also exhibit rich phases and phase transitions [36].

Although there are some reviews focusing on 2D ferroelectrics [8] and their applications, [11], there are few literatures focusing on phase transitions of 2D ferroelectrics. At the same time, the concepts of Moire ferroelectricity and sliding ferroelectricity associated with interlayer phase transitions remain elusive. One of the most critical challenges facing 2D ferroelectrics is the presence of numerous coexisting ferroelectric and non-ferroelectric phases that remain unidentified or elusive. Clarifying the structures, stability, and phase transition mechanisms of 2D ferroelectrics remains challenging, while insufficient phase control hinders the scalable synthesis and application of these materials. Therefore, there is a crucial need to study and summarize methods for additional phase control in 2D ferroelectrics, which could lead to the discovery of more ferroelectric materials and their applications in the future.

This review focuses on the additional facile phase control in 2D vdW ferroelectrics beyond temperature-induced ferroelectric phase transitions. We present state-of-the-art discoveries in 2D ferroelectrics in recent years, including intrinsic and extrinsic ferroelectrics. We summarize large-area preparation methods for 2D ferroelectric films under the guidance of phase transition. Furthermore, we also discuss various approaches and external stimuli for phase control in 2D ferroelectrics, including

strain, electric fields, and twisted angles. In addition, we briefly examine *in situ* experimental techniques for investigating phase transitions. The underlying phase transition mechanisms, in particular, the Moiré ferroelectricity and sliding ferroelectricity are elaborated. We demonstrate new device applications that combine phase control and ferroelectricity. Finally, we provide an overview of the challenges and future research perspectives on 2D ferroelectric phase control.

2. 2D ferroelectrics

Ferroelectric materials can undergo changes in their crystal and electronic structures in response to external electric, magnetic, or thermal fields. At the point of a first-order phase transition, latent heat is involved, while second-order phase transitions result in gradual changes in physical properties near T_c. The essential difference between the two is that second-order phase transitions do not involve latent heat, whereas first-order phase transitions typically do. It is worth noting that most 2D ferroelectric phase transitions are first-order phase transitions [27, 37].

2.1. 2D intrinsic ferroelectrics

Up to present, the room temperature (RT) 2D intrinsic ferroelectrics that have been experimentally demonstrated include SnTe ([10, 38]), $MoTe_2$ ([39–41]), WTe_2 ([42]), In_2Se_3 ([43–45]), $CuInP_2S_6$ ([46, 47]), SnSe ([48]), SnS ([49]), MoS_2 ([50]), ReS_2 ([51].), GaSe ([52]), Ga_2Se_3 ([53]), Bi_2O_2Se ([54].), $CuCrS_2$ ([55]), $Cd_7Te_7Cl_8O_{17}$ ([56]), InSe ([57]), BA_2PbCl_4 ([58]), $NbOI_2$ ([59]), $Bi_2Te_2O_5$ ([60]), GeTe ([61]), and $CuCrP_2S_6$ ([62]). Meanwhile, other 2D materials exhibiting ferroelectricity under RT have also been explored, such as NiI_2 ([63]) and Bi monolayer ([64]). The main properties of 2D vdW ferroelectrics are listed in table 2. The milestones are discussed below.

Origin of spontaneous polarization. Spontaneous polarization arises from the shifting of atomic positions, or the charge redistribution. Actually, there are other mechanisms, such as polar molecular and spin texture driven polarization, not discussed here. As depicted in figure 1(a), α-In_2Se_3 shows the Se–In–Se–In–Se quintuple layers, and its interlocked out-of-plane (OOP) and in-plane ferroelectricity stems from the movement of Se atoms in the central layer. Furthermore, its ferroelectricity can be maintained to the monolayer limit [71–73]. The polarization switch in α-In_2Se_3 by the external electric field is also a structural phase transition occurring through the movement of the Se atoms. Likewise, bilayer T_d-$MoTe_2$ possesses non-centrosymmetric degenerate ground states, and the shifting of layers with mirror operation results in the polarization switch [39, 68]. In SnTe, at the ferroelectric transition temperature T_c, Sn and Te atoms slightly shift along the [74] direction, achieving the polarizable ferroelectric phase [38]. In bilayer WTe_2, the polarization originates from vertical charge transfer by slight interlayer sliding, and the reversed polarization arises from mirror operation as well.

Curie temperature of 2D intrinsic ferroelectrics. 2D ferroelectrics will undergo intrinsic ferroelectric phase transition at Curie temperature (T_c). Ferroelectricity exists only below T_c, while above T_c the spontaneous electric polarization vanishes and leads to the paraelectric phase, as shown by the P_s–T curve in figure 1(b). Some 2D intrinsic ferroelectrics that have been experimentally proven to date exhibit Curie temperatures above RT, as illustrated in figure 1(c).

Milestones of 2D intrinsic ferroelectrics development. Since 2016, researchers have made significant efforts in controlling the phases of 2D intrinsic ferroelectrics, resulting in several major breakthroughs and milestone works in this area. The first experimental study of in-plane 2D ferroelectricity in 0.6 nm thick (1 unit cell, 1 UC) SnTe was reported and its temperature-controlled second-order ferroelectric phase transition was studied [10]. Notably, the ferroelectric phase transition temperature (T_c) of 1-UC SnTe reaches 270 K compared with the 98 K T_c of bulks. Besides, the 2–4 layers of SnTe also exhibit RT ferroelectricity. At Curie temperature, SnTe undergoes a cubic to rhombic structural phase transition, where the two sublattices of Sn and Te atoms shift towards each other in the direction [74], producing a polarization state. The robust RT ferroelectricity in 2D SnTe can potentially enable a wide range of applications in non-volatile high-density memories, such as ferroelectric random-access memory devices.

TMDs with MX_2 chemical formula (M = Mo, W; X = Se, Te, S) are important layered materials with rich phases and phase transitions. Among them, $MoTe_2$ has phases of semiconducting 2 H phase, metallic 1 T′ phase, and ferroelectric Td phase (figure 1(d)). Monolayer Td-$MoTe_2$ has been suggested to exhibit room-temperature OOP ferroelectricity confirmed by PFM, SHG, and TEM. The ferroelectricity is resulted from the symmetry breaking by atomic displacements of Mo and Te atoms [39]. Its ferroelectric appliances also exhibit a large ON/OFF resistance ratio. This is also the first report of room-temperature ferroelectricity found in monolayer $MoTe_2$, which provides a basis for the study of other TMD materials. The electrostatic-doping-driven reversible phase transition between 2 H and 1 T′ monolayer $MoTe_2$ evidenced by *in situ* Raman and second-harmonic generation (SHG) spectroscopy was reported [40]. This kind of electrostatic-doping-driven phase transition by ionic liquid will show great application potentials in

Table 2. The main properties of 2D vdW ferroelectrics.

Material (ref.)	Polarization direction	T_c (K)	P (μC cm^{-2})	Twisted angle (°)	References
α-In_2Se_3	IP, OOP	4 l, 700	1 l, 2.14; Bulk, 11.34	/	[43–45]
$CuInP_2S_6$	OOP	5 l, >320	3.5	/	[46, 47]
SnTe	IP	1 l, 270; Bulk, 100	1 l, 22	/	[10, 38]
SnSe	IP	1 l, >380	1 l, 18.1 ^{T}	/	[48]
SnS	IP	1 l, >300	1 l, 26 ^{T}	/	[49]
3 R-MoS_2	OOP	2 l, 650	1 l, 0.23 ^{T}	/	[50]
d1T-$MoTe_2$	OOP	1 l, 330	1 l, 0.1 ^{T}	/	[39–41]
T_d-WTe_2	OOP	2–3 l, 350	0.2 pC m^{-1}	/	[42]
1 T′-ReS_2	OOP	2 l, 405	2 l, 0.07 pC m^{-1} (T)	/	[51]
GaSe	IP, OOP	1 l, >300	1 l, 4.89 pC m^{-1} (T)	/	[52]
Ga_2Se_3	IP, OOP	4 l, 450	/	/	[53]
Bi_2O_2Se	OOP	3 l, 508	1 l, 284 pC m^{-1} (T)	/	[54]
$CuCrS_2$	IP, OOP	4 l, 500	/	/	[55]
InSe	IP, OOP	50 nm, >300	Bulk, 0.08	/	[57]
BA_2PbCl_4	IP	2 l, >300	13	/	[58]
$NbOI_2$	IP	6 l, >300	Bulk, 50	/	[59]
$Bi_2Te_2O_5$	IP	>300	5.57 (T)	/	[60]
GeTe	IP	1 l, 570 (T)	1 l, 32.8	/	[61]
NiI_2	IP	1 l, 21; Bulk, 59.5	0.0125	/	[63]
Bi	IP	1 l, 4.3	/	/	[64]
$CuCrP_2S_6$	OOP	4 l, 333	Bulk, 16.05	/	[62]
Twisted bilayer h-BN	OOP	2 l, >300	2.25 pC m^{-1}	0.24 ∼ 0.5	[65–67]
WSe_2, $MoSe_2$, WS_2, MoS_2	OOP	2 l, >300	2.0 pC m^{-1}	0.25 ∼ 2	[68, 69]
Heterobilayer WS_2/MoS_2	OOP	2 l, >300	1.45 pC m^{-1}	0	[70]

P, polarization; T, theoretical calculation; IP, in-plane; OOP, out-of-plane; L, layer; /, unconfirmed; *d*, distorted.

ferroelectric phase change memory and biomimetic neuromorphic computing devices.

The discovery of room-temperature ferroelectricity in semimetal has opened up possibilities for its use in ferroelectric devices. Expanding on this research, Hou *et al* reported a ferroelectric phase-change field-effect transistor based on $MoTe_2$, which leveraged electric-field-induced strain engineering to enable ultrafast, low-power, non-volatile logic and memory devices [41]. Ferroelectricity usually occurs in semiconductors or insulators, and is rarely found in metals. However, the spontaneous OOP electric polarization and ferroelectric switching in bilayer and trilayer topological semimetal WTe_2 was discovered [42]. Using graphene as an electric-field sensor, they also quantitatively measured the polarization intensity of 2D WTe_2.

From the Landau–Ginzburg theory, ferroelectric generally has two potential-energy minima corresponding two polarization states. In another 2D intrinsic ferroelectric, $CuInP_2S_6$ possesses four local energy minima. The coexistence of four polarization states in $CuInP_2S_6$ and the temperature-, pressure- and bias-dependent ferroelectric phase transitions were found [46]. They use piezoresponse force microscopy (PFM) data to reveal an unconventional ferroelectric property, a uniaxial quadruple potential well for Cu displacements in $CuInP_2S_6$, which is capacitated by the vdW gap. The four-well potential is structurally caused by the instability of Cu, which can occupy one or several sites (such as Cu1, Cu2, and Cu3) under temperature, strain and bias. Firstly, at temperature above T_C of 315 K, the Cu ions are highly mobile and can occupy sites at interlayer and intralayer, revealing a spatial disorder of Cu. For strain factor, at low polarization state, the Cu ions are very sensitive to strain, and the compression of the lattice along the interlayer direction can cause the displacement of Cu away from the In position. For bias activating, the Cu ions can be electrically displaced from its equilibrium Cu1 position into the vdW gap, which has a second stable position. The change caused by this displacement is from a structure with two low polarization minima to that with two additional high polarization minima. The Cu ions can partially movesinto the vdW gap and bond with the S atom across the gap, doubling the polarization value.

In addition to their potential use in electronic devices, the phase transitions of 2D ferroelectrics, such as in In_2Se_3, have shown significant promise for phase control during materials synthesis. The energy barrier of different phases (α, β, β' and γ) is low, so it is easy to transition between different phases (figure 1(d)) [35]. Very recently, we have investigated the phase-transition mechanisms of ferroelectric α-In_2Se_3 and antiferroelectric (AFE) β'-In_2Se_3, and successfully obtained the large-area ferroelectric α-In_2Se_3 films by inducing the $\beta' \rightarrow \alpha$ phase transition in 2D In_2Se_3 [43, 44]. We also investigated the phase transition mechanisms between the three phases (α, β' and γ) by means of *in-situ* TEM and introducing different stimulation methods, including thickness, strain, and Joule heat. The revelation of the phase

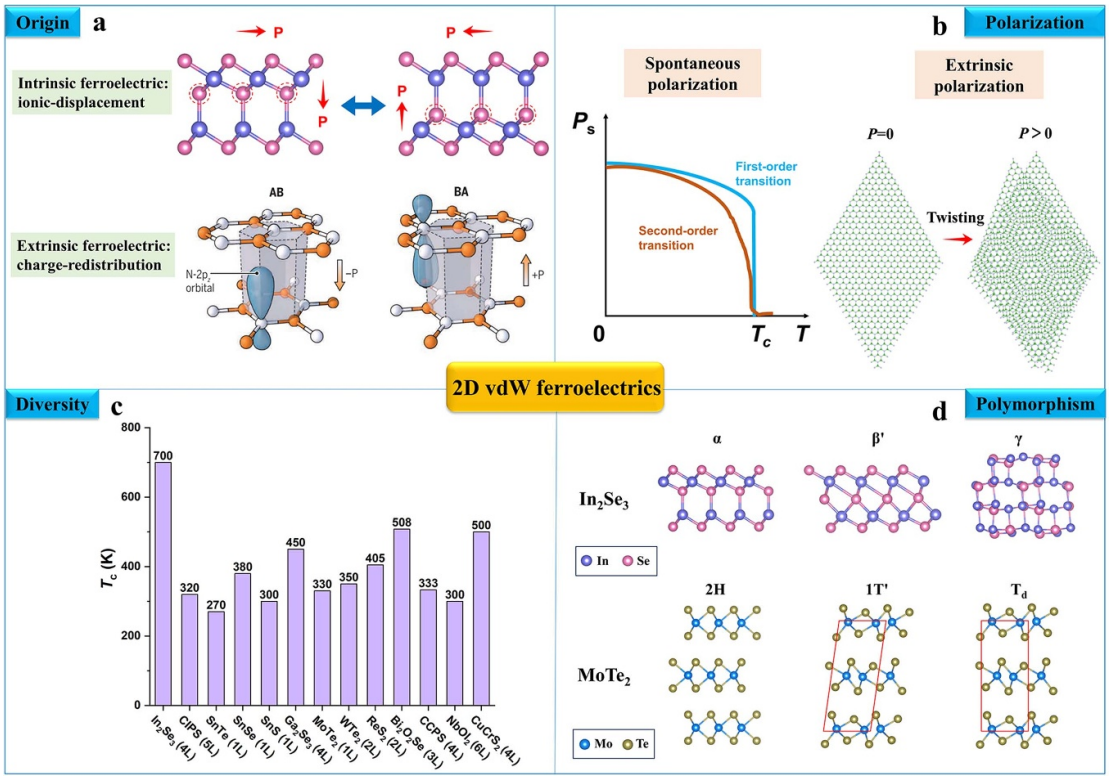

Figure 1. Polarization and polymorphism of 2D vdW ferroelectrics. (a) Origins and mechanisms of spontaneous polarization in 2D intrinsic and extrinsic ferroelectrics. In 2D intrinsic ferroelectrics, ionic-displacement is responsible for the spontaneous electric polarization. In 2D extrinsic ferroelectrics, charge-redistribution is in charge of the extrinsic electric polarization. (b) P_s–T curve in 2D intrinsic ferroelectrics. P_s: spontaneous electric polarization. T: temperature. T_c: Curie temperature. The right part is a schematic diagram of polarization intensity from $P = 0$ to $P > 0$ after twisting in 2D extrinsic ferroelectrics. (c) The curie temperature histograms of 13 experimentally confirmed 2D intrinsic ferroelectrics with corresponding number of layers. In_2Se_3 ([45].), $CuInP_2S_6$ ([47].), SnTe ([10].), SnSe ([48].), SnS ([49].), Ga_2Se_3 ([53].), $MoTe_2$ ([39].), WTe_2 ([42].), ReS_2 ([51].), Bi_2O_2Se ([54].), $CuCrS_2$ ([55].), $NbOI_2$ ([59].), and $CuCrP_2S_6$ ([62].).(d), the crystal structures of α, β, and γ phases of In_2Se_3 and the 2 H, 1 T′, and T_d phases of $MoTe_2$. From [67]. Reprinted with permission from AAAS.

transition mechanisms lays a foundation for the controlled growth and device application of 2D In_2Se_3.

2.2. 2D extrinsic ferroelectrics

Except from the intrinsic 2D ferroelectrics, depending on the stacking order, 2D vdW bilayers can exhibit polarized states by assembly of non-ferroelectric materials, as seen in h-BN and TMDs, which we call 2D extrinsic ferroelectrics. The high-density ferroelectric domains in these bilayers can be effectively controlled using electric fields or mechanical strain, including twist torque. Ferroelectricity has been recently experimentally uncovered in a series of 2D moiré superlattices and heterostructures through extrinsic stack engineering designed to break the inversion symmetry. With the discovery of magic-angle graphene superlattices, [69] the concept of 'twisted-angle' was also introduced into the field of ferroelectricity. Thus, ferroelectricity can be artificially created in stacked moiré superlattices of 2D layers.

Break of stacking symmetry and interlayer charge transfer. In natural or assembled 2D bilayer, the transfer of interlayer charges through hybridization between occupied states in one layer and unoccupied states in adjacent layers can cause an OOP electric dipole. The physical essence of twisted-ferroelectricity, interfacial-ferroelectricity and sliding- ferroelectricity proposed at present is interlayer-charge-transfer induced polarization or charge-redistribution induced polarization. For instance, the emergent moiré ferroelectricity and odd-parity electronic ordering in graphene-based moiré heterostructures (hBN/BLG/hBN) was first reported [75]. In 2021, Yasuda *et al* [65] and Stern *et al* [66] reported the successful engineering of interfacial ferroelectricity in hBN layers by artificially stacking the parent non-polar compound. They proposed the phase-change mechanism involves an artful interaction between charge redistribution and ionic displacement (figure 1(a) down panel) [67]. In 2022, two research groups [68, 69] independently demonstrated the existence of interfacial ferroelectricity in stacked bilayer TMDs, including WSe_2, $MoSe_2$, WS_2, and MoS_2. In another work, we reported the OOP ferroelectricity and piezoelectricity in untwisted MoS_2/WS_2 heterobilayers arising from symmetry breaking and interlayer sliding [70]. Furthermore, Deb *et al* reported that the parallel WSe_2 and MoS_2

multilayers revealed multiple polarization states and 'ladder-ferroelectrics' by a cumulative interfacial effect [76].

New phase transition mechanisms revealed in 2D extrinsic ferroelectrics. 2D extrinsic ferroelectrics typically undergo a ferroelectric phase transition at critical twisted angle or/and stacked layers (N_c). N_c means the number of the stacked layer, including two aspects, one is twisted three layers or more of the same material and another is the total number of layers of heterogeneous stacking. Ferroelectricity exists only above N_c, as shown by the P_s–N curve in figure 1(b). AA′ layer stacking in bilayer hBN makes h-BN non-polar. AB or BA stacking can produce an OOP electric dipole with polarization oriented downward or upward, respectively [65–67]. For Rhombohedral (R)-stacked bilayer TMDs, by breaking the OOP mirror symmetry, an OOP polarization ($-P$ or $+P$) arises due to the vertical alignment of different types of atoms [77, 78]. Other 2D moiré superlattices and heterostructures exhibiting ferroelectricity at RT have also been investigated, such as hBN/BLG ([75].), WSe_2/BP ([79].), MoS_2/WS_2 [70] and WTe_2/WSe_2 ([80].).

Furthermore, we have recently made significant progress in understanding the phase transition mechanisms in vdW InSe and other metal monochalcogenide layers. Our research has revealed a more comprehensive phase transition that involves both intralayer atomic reorganization (close to intrinsic) and interlayer stacking reorganization (close to extrinsic). Notably, we have discovered that mechanical stimuli can induce these phase transitions in vdW InSe and similar metal monochalcogenide layers ([81].). The study of ferroelectric behavior in these metal monochalcogenides ([52].) presents a more complex and intriguing phenomenon that is currently being investigated.

3. Scalable synthesis of 2D ferroelectrics

The scalable synthesis and phase engineering of 2D ferroelectrics are crucial for their application in various fields.

2D ferroelectrics have great potential for future devices. However, the shift of 2D ferroelectrics from lab to fab is still in its infancy, and meeting industrial requirements and reproducible manufacturing standards has been a big challenge. We summarized the current growth status of several representative 2D intrinsic ferroelectric materials, including growth size and method (table 3). At present, only MoS_2 can reach the industrial-scale 12 inch, and good performance and repeatability [81]. Other 2D ferroelectrics still require long periods of trial and error. Are there particular methods that appear promising? From the current experience with MoS_2, it seems that metal-organic chemical vapor deposition (MOCVD) is a promising approach for other 2D ferroelectrics.

Table 3. Growth size and method of 2D vdW ferroelectrics.

Material	Size (mm)	Method	References
MoS_2	300	CVD	[82]
$MoTe_2$	25	CVD	[83]
In_2Se_3	10	CVD	[43]
WTe_2	10	ALD + CVD	[84]
SnS	50	CVD	[85]
SnSe	150	CVD	[86]
SnTe	50	CVD	[87]
Bi_2O_2Se	3	CVD	[88]

Growth of MoS_2. Although 2H-MoS_2 is non-ferroelectric, the transition to a ferroelectric phase can be achieved through phase transitions, twisting, or 3 R stacking enginerring. 8 inch monolayer MoS_2 is already available by low-thermal-budget MOCVD method with a growth temperature less than 300 °C, which can meet the temperature requirements of the silicon back-end-of-line (BEOL) integration process [82]. Despite MOCVD's advantages, because inorganic CVD has advantages over MOCVD in terms of cost and safety, researchers have still been exploring growing wafer-scale monolayer MoS_2 through inorganic precursors. They ensured uniform growth of single-layer MoS_2 by pre-depositing a layer of amorphous Al_2O_3 on a 12 inch silica substrate and releasing the precursor in a controlled manner [82]. The MoS_2-based transistor arrays show excellent performance, which provides the basis for the construction of industrial pilot lines. More importantly, through phase engineering, twisting engineering, stacking engineering, ferroelectric phase MoS_2 can be obtained, even with a size of 12 inch. For example, by twisting 2 pieces of MoS_2 film at a small angle, so as to obtain 12 inch of ferroelectric film.

Growth of $MoTe_2$. The preparation of large-area single-crystal film is the key to the practical application of 2D ferroelectrics. Utilizing the phase transition mechanism to synthesize 2D ferroelectric films has recently become effective. As depicted in figure 2(b), The CVD growth of 1 inch wafer-scale single-crystalline 2 H $MoTe_2$ films on an insulating substrate by a seeded epitaxy method was reported [83]. Unlike traditional CVD, they grew the 2D $MoTe_2$ films in a confined space by a solid-to-solid phase transition and recrystallization process. First, they obtained polycrystalline 1 T′ $MoTe_2$ film, and then transferred a 2 H $MoTe_2$ seed crystal onto the film. Afterward, 30 nm Al_2O_3 film was deposited on the wafer by atomic layer deposition (ALD) to separate the Te gas (figure 2(b)). Next, a small hole was made in the seed to introduce Te gas. Thus,

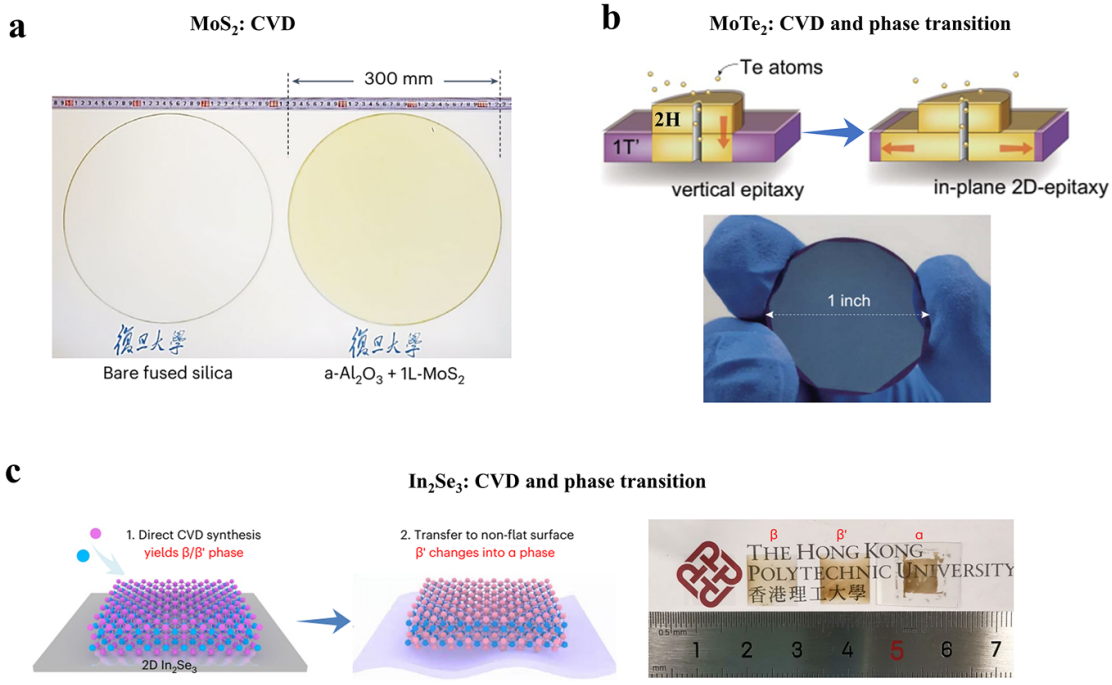

Figure 2. Scalable synthesis and phase engineering on 2D ferroelectrics. (a) Photo of two 12 inch wafers of bare fused silica substrate and monolayer MoS_2 growth. (b) Up panel, schematic for the phase-transition growth of wafer-scale single-crystalline 2 H $MoTe_2$ film. Down panel, OM image of 1 T′/2 H interface, and photo of 1 inch $MoTe_2$ wafer. (c) Up panel, schematic of the CVD-based synthesis of β-, β'- and α-In_2Se_3 films. The β and β' phases can be grown by CVD and the α phase can be prepared by transferring the β' phase to non-flat surface. Down panel, photograph of the large-area In_2Se_3 films with three phases. Panel (a) Reproduced from [82], with permission from Springer Nature. Panel (b) From [83]. Reprinted with permission from AAAS. Panel (c) Reproduced from [43], with permission from Springer Nature.

the in-plane 2 H/1 T′ $MoTe_2$ heterophase junctions were obtained after vertical epitaxy. Subsequently, phase transition and recrystallization started from this heterophase, ultimately leading to the growth of a single crystal 2 H $MoTe_2$ film via in-plane 2D-epitaxy.

Growth of In_2Se_3. Most of the 2D ferroelectrics are difficult to grow directly, such as T_d-$MoTe_2$, α-In_2Se_3, etc. If the phase transition mechanism between ferroelectric and non-ferroelectric phases is understood, subsequent phase engineering can indirectly synthesize the ferroelectric phase. Very recently, we reported the CVD-based phase-controllable synthesis of large-area single-crystalline In_2Se_3 films with three phases and a hetero-phase junction by manipulating the vacancy and strain, as shown in figure 2(c) [43]. First, a short-distance CVD method is used to grow centimeter-size β-In_2Se_3 film using In_2O_3 and Se powder as precursors. The short distance between precursor and substrate can provide a stable and uniform concentration supply of indium source. After introducing β-InSe powder to In_2O_3 as the mixed precursor, the films on mica show different Se/In ratios and Se vacancy concentrations, realizing the transformation from β to β' phase. β-InSe may serve two roles during the CVD growth of In_2Se_3 films: changing the Se vacancy and acting as a seed to promote the growth of the β' phase. After transferring the β'-In_2Se_3 films onto non-flat surface like PET or Au-coated silicon, the in-plane strain will release and the β'-In_2Se_3 phase will transform to α-In_2Se_3 phase. The phase transition was utilized to produce an in-plane α–β' hetero-phase junction with a ferroelectric–antiferroelectric configuration, which improved non-volatile memory device performance.

In summary, for large-scale 2D instrinsic ferroelectrics growth, such as WTe_2 [84], SnS [85], SnSe [86], and SnTe [87], by the CVD or ALD + CVD method, they can obtain a size of more than 10 mm (figure 2(d)). For the ternary compound, Bi_2O_2Se can only be obtained in a maximum size of 3 mm by CVD [88]. Regarding other 2D ferroelectrics, it is worth noting that their growth sizes are currently limited to the micron meter scale. Therefore, extensive research and exploration in this field are still necessary to advance our understanding and unlock their full potential.

4. External stimuli for phase transition in 2D ferroelectrics

External stimuli have been identified as means of controlling the phases and ferroelectricity of 2D materials. Currently, a range of external stimuli that can trigger phase transitions have been studied in 2D ferroelectrics, including strain, electric field, electrostatic gating, electric current, temperature/laser, defect,

Table 4. The main phase transitions and trigger factors in 2D ferroelectrics.

Phase A → Phase B	2D ferroelectrics	Trigger factors	References
$\alpha \rightarrow \beta'$	In_2Se_3	Temperature, electric current, strain, thickness	[43, 44]
$\beta' \rightarrow \alpha$		Strain, thickness	[43, 44]
$\beta \rightarrow \beta'$		Defect	[43]
$\alpha \rightarrow \gamma$, $\beta' \rightarrow \gamma$		Electric current	[44]
2 H → 1 T′	$MoTe_2$	Electrostatic doping, electric field, laser, defect, strain, hot electrons, e-beam, temperature	[40]
	MoS_2	Electrostatic doping, e-beam	[27]
1 T′ → 2 H	$MoTe_2$	Electrostatic doping, electric field, strain	[40]
	MoS_2	Electrostatic doping	[27]
1 T′ → T_d	$MoTe_2$	Temperature	[89–92]
2 H → T_d	$MoTe_2$	Dimensionality	[93]
Normal → superconductor	$MoTe_2$	Temperature	[39]
Cubic → rhombohedral	SnTe	Temperature	[10]
LP ↔ HP	$CuInP_2S_6$	Temperature, pressure, and bias	[47]
Monoclinic → trigonal		Thickness	[94]
R3m → Cm	GeTe	Electric-field, temperature	[61]
Pc→C2/c	$CuCrP_2S_6$	Temperature, spin	[63]
AFE → FE	SnS, SnSe	Reduced dimensions, temperature	[48, 49]
	GeSe	Electric-field, temperature	[95]
PE → FE	WTe_2	Interlayer charge transfer	[42]
	Ga_2Se_3	Defect	[53]
	ReS_2, GaSe, InSe	Interlayer sliding, interlayer charge transfer	[51, 52, 57]
	MoS_2	Mechanical pressure, thickness	[50]
	BA_2PbCl_4, NiI_2, $NbOI_2$, Bi_2O_2Se, $Bi_2Te_2O_5$, $Cd_7Te_7Cl_8O_{17}$, $CuCrS_2$	Temperature	[54–56, 58–61]
	Bi	Thickness	[64]
	hBN/BLG	Moiré superlattice potential, twisted angle	[75]
	hBN/hBN	Twisted angle, stacking, interfacial ferroelectrics	[65–67]
	WSe_2/BP, WTe_2/WSe_2	Stacking	[79, 80]
	TMD/TMD	3 R stacking, interfacial ferroelectrics, interlayer charge transfer	[77, 78]
	MoS_2/WS_2	Heteroepitaxy, symmetry breaking, interlayer sliding	[70]

Notes: AFE: antiferroelectric; FE: ferroelectric; PE: paraelectric; LP: low polarization; HP: high polarization; BLG: bilayer graphene; BP: black phosphorus; TMD: transition metal dichalcogenides.

twisted-angle, stacking, etc. We have summarized the major phase transitions and the external stimuli in 2D ferroelectrics, as listed in table 4.

Strain-induced transition. A strain-release induced $\beta' \rightarrow \alpha$ phase transition in 2D In_2Se_3 film has been recently discovered [43, 44, 96, 97], as depicted in figure 3(a). After transferring the CVD-grown 2D β'-In_2Se_3 film from mica onto flexible substrates (PET, etc.) or non-flat substrates (gold-particles-patterned SiO_2/Si), the β'-In_2Se_3 film can be transformed to α-In_2Se_3 film through a complete phase transition. The $\beta' \rightarrow \alpha$ phase transition mechanism has been investigated by density functional theory (DFT) calculations, *in situ* Raman and *in situ* TEM, confirming the film delamination and interfacial strain release [52, 53]. Upon phase transition, a lot of wrinkles appeared in the α-In_2Se_3 film due to the

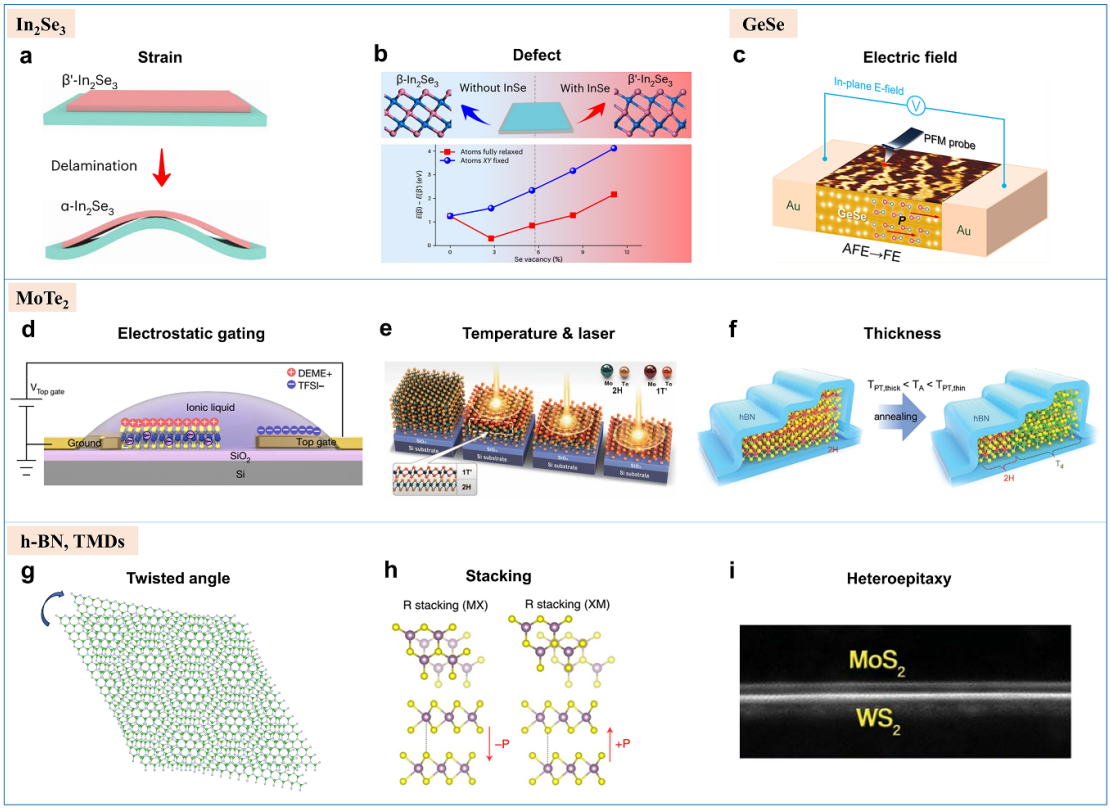

Figure 3. External stimuli that can drive the phase transitions in 2D ferroelectrics. (a) Strain driven $\beta' \rightarrow \alpha$ phase transition in 2D In_2Se_3. (b) Defect induced $\beta \rightarrow \beta'$ phase transition in 2D In_2Se_3. (c) Electric-field triggered AFE → FE phase transition in 2D GeSe. (d) Electrostatic-gating induced 2 H↔1 T′ phase transition in 2D $MoTe_2$. (e) Temperature/laser induced 2 H → 1 T′ phase transition in 2D $MoTe_2$. (f) Thickness-driven 2 H → T_d phase transition in 2D $MoTe_2$. (g), Twisted-angle induced PE → FE phase transition in hBN/hBN Moiré superlattice. (h), Interfacial polarization induced PE → FE phase transition in hBN layers. (i) Stacking/heteroepitaxy induced PE → FE phase transition in MoS_2/WS_2 heterostructures. Panel (a) and (b) Reproduced from [43], with permission from Springer Nature. Panel (c) Reprinted with permission from [95] Copyright (2022) American Chemical Society. Panel (d) Reprinted with permission from [40]. Copyright (2017) American Chemical Society. Panel (e) From [97]. Reprinted with permission from AAAS. Panel (f) [93] John Wiley & Sons. © 2021 Wiley-VCH GmbH. Panel (g) From [67]. Reprinted with permission from AAAS. Panel (h) Reproduced from [77], with permission from Springer Nature. Panel (i) From [70]. Reprinted with permission from AAAS.

delamination process. From the *in situ* TEM study by piezo-driven nanomanipulator, the phase transition process has been observed and captured, which proves the strain relaxation in the compression-relaxation process. The $\alpha \rightarrow \beta'$ phase transition in 2D In_2Se_3 film has been achieved by tensile strain inside TEM as well. Therefore, a complete and reversible phase/polarization transition process ($\beta' \rightarrow \alpha \rightarrow \beta'$) can be realized on the same 2D In_2Se_3 sample.

The strain-induced polarization transition was also observed in 2D MoS_2 [98]. Lipatov *et al* reported a stable room-temperature OOP polarization ordering and switching in 2D MoS_2 flakes by applying mechanical pressure with an atomic force microscope (AFM) tip. Ferroelectric MoS_2 exhibits a 1 T″ phase with a distorted trigonal structure. As another member of 2D TMDs, $MoTe_2$ is a typical polymorphic material, including 2 H, 3 R, 1 T, 1 T′, and 1 T_d phases [99]. Compared with other TMDs, the energy difference between the 2 H phase and 1 T′ phase of $MoTe_2$ is much smaller (∼35 meV), which makes it convenient for the phase transition of 2 H ↔ 1 T′ by various external stimuli [100]. By applying/releasing a small tensile strain of 0.2% by AFM tip, the reversible 2 H ↔ 1 T′ phase transition in $MoTe_2$ flakes was realized [101]. Inspired by this principle, Wu *et al* reported a $MoTe_2$-based phase-change field-effect transistor using strain engineering, highlighting its potential for use in low-power, non-volatile, and fast-switching memory devices [41].

Defect-induced transition. For the CVD growth of 2D In_2Se_3, we found that by adding β-InSe powder into the In_2O_3 precursor, the AFE β'-In_2Se_3 films can be readily obtained [43]. While without β-InSe precursor, we can only acquire PE β-In_2Se_3, as shown in figure 3(b). According to the DFT calculations, the stability of the β' phase can enhance with the increasing Se vacancy concentration. Thus at high temperatures, the Se deficiency can transform the β-InSe into β'-In_2Se_3. Through a combination of experimental evidence and theoretical calculations, a route for growing continuous β'-In_2Se_3 films based

on the vacancy-promoted $\beta \rightarrow \beta'$ phase transition and the seed effect has been identified.

Electric-field-induced transition. The electric field is an effective means for flipping the polarization of 2D ferroelectrics and can stimulate their phase transitions, as shown in figure 3(c). Orthorhombic GeSe bulk is experimentally shown to be an intrinsic AFE material without the net polarization, and with a high T_c of 700 K [95]. Theoretical calculations have suggested that the AFE state in GeSe represents the lowest energy state. The FE state ($+P_y$ and $-P_y$) is metastable, and their energy difference is 4.39 meV per atom. Triggered by an external in-plane electric field, a reversible AFE to FE phase transition at RT in 2D GeSe was realized, as confirmed by *in situ* PFM and SHG measurements.

Similarly, in 2D $MoTe_2$, the small energy difference between 2 H and 1 T phases makes the phase transition prone to occur. In the vertical 2 H-$MoTe_2$- and $Mo_{1-x}W_xTe_2$-based memory devices, Appenzeller *et al* reported the electric-field-induced phase transition from 2 H to 2 H_d and T_d phases [102]. This controlled electric switch by phase transition shows the potential of 2D resistive random-access memory (RRAM) devices.

Electrostatic-gating-induced transition. Electrostatic gating and ion intercalation is another efficient way to excite the phase transitions of 2D ferroelectrics [30]. Reed *et al* predicted that electrostatic-gating could trigger the semiconductor-to-semimetal phase transitions in 2D TMDs, such as MoS_2 and $MoTe_2$ [103]. By electrostatic-gating using an ionic liquid, Wang *et al* reported the phase transition between 2 H and 1 T′ monolayer $MoTe_2$ evidenced by *in situ* Raman and SHG spectroscopy (figure 3(d)) [40]. The gate voltage reverses the phase transition and exhibits a hysteretic loop in Raman spectra. This electrostatic-gating-driven phase transition has the potential to enable new phase-change devices of 2D materials. In 2019, a reversible 2 H-1 T′ phase transition in MoS_2 by Li^+ ions electrostatic-gating was realized [104]. The local 2 H-1 T′ phase transition of MoS_2 by controlling the migration of Li^+ ions under an electric field can lead to the resistance change in the 2D MoS_2 layer. The increase or decrease of local Li^+ ions concentration results in the MoS_2 resistive switching between the metallic state (1 T′ phase, low resistance state) and the semiconducting state (2 H phase, high resistance state). The high in-plane diffusion rate of Li^+ ions enable efficient ion coupling through a local ion exchange in multiple MoS_2 devices, which is similar with the synaptic competition and synaptic cooperation effects in bio-inspired artificial neural networks.

Temperature/laser-induced transition. Temperature is one of the most important factors leading to phase and polarization transitions. 2D ferroelectrics not only can undergo a ferroelectric phase transition above the Curie temperature, but also other thermal-induced or laser-induced phase transitions may occur, such as in $MoTe_2$ and In_2Se_3. Bulk $MoTe_2$ possesses a reversible temperature-induced structural phase transition between 2 H- and 1 T′ phases [96]. In 2015, we reported the laser-induced 2 H $\rightarrow$ 1 T′ structural phase transition in 2D $MoTe_2$ flakes (figure 3(e)) and the ohmic hetero-phase homojunction devices, significantly improving carrier mobility [97]. Using *in situ* TEM study, we proposed that Te vacancy can induce local phase transition in $MoTe_2$. Besides, the temperature-driven phase transitions between 1 T′ and the ferroelectric Td $MoTe_2$ phases are also reported [89–92]. For the bulk, the 1 T′ phase transitions to T_d phase at ∼250 K by inversion symmetry breaking. Different from the phase transition temperature of bulk 1 T′-$MoTe_2$, the temperature-driven phase transition is gradually inhibited with thickness decreasing. Even at the same thickness, the phase transition and critical temperature of different samples are significantly different, which may be due to the atomic defects or local strain [93].

For In_2Se_3, due to the small energy difference between α, β and β' phases, the phase transitions can occur at relatively low temperatures. The $\alpha \rightarrow \beta$ transition temperature ranges from 550 to 650 K with decreasing thickness of In_2Se_3 flakes [98]. Furthermore, the $\alpha \rightarrow \beta$ transition can be triggered by ordinary laser or nanosecond laser pulse to fabricate in-plane α–β heterostructures for photodiode and integrated photonic memory devices [99, 100]. In the study of Joule-heat-induced transition, by using *in situ* electrical TEM approach, we realized the phase transitions among the FE α-In_2Se_3, AFE β'-In_2Se_3 and PE γ-In_2Se_3 [44]. When the tungsten tip contacts the 2D In_2Se_3 films, the current produces Joule heat locally near the tip. As a relatively low current is applied, α-In_2Se_3 can transform into β'-In_2Se_3. When a higher current is applied, α-In_2Se_3 can directly transform into γ-In_2Se_3. Here, the controllable phase and ferroelectric polarization in 2D In_2Se_3 can be a valuable guide for exploring the phase transitions in other 2D ferroelectrics.

Thickness-induced transition. Compared to the bulk or 3D materials, 2D materials can reach an atomic-level thickness, even by a simple Scotch-tape exfoliation. Dimensionality reduction from 3D to 2D results in physical property changes (e.g. Curie point), mechanical property changes (e.g. OOP bending), and makes 2D materials more sensitive to external fields. 2D vdW ferroelectrics are also different from conventional ferroelectrics. For instance, bulk SnS is centrosymmetric. As the thickness is thinned down to several layers, the centrosymmetric is preserved in the even-number-layer SnS flake, but is removed in the odd-number-layer SnS flake, creating in-plane

polarization [36]. The ferroelectricity in monolayer group-IV monochalcogenides MX (M = Ge, Sn; X = S, Se) was predicted and part were experimentally verified. The thickness-dependent relation of spontaneous polarization and odd-number-layer of MXs reveals that the polarization intensity decreases with the increase of the number of layers. The thickness-dependent effect is also found in 2D In_2Se_3 [44]. When the number of layers is equal to or greater than 4 layers, In_2Se_3 maintains a β'-phase. In contrast, when the number of layers is less than 4, the super-spots in the SAED pattern disappear, showing a phase transition from β'-In_2Se_3 to α-In_2Se_3. Thus, dimension or layer number, as an important parameter, is also one of the mechanisms causing 2D ferroelectric phase transformation. The room-temperature sliding ferroelectricity in 2D 1 T′-ReS_2 was verified by experiment with number of layers more than one [51]. However, when the thickness is reduced to a single layer, its ferroelectric property disappears and becomes a non-ferroelectric phase. This may be due to the fact that reversing symmetry in the monolayer prevents polarization from occurring.

Due to the large-specific-surface-area and quantum confinement effect, the phase transition of 2D materials is very different from that of bulk materials. For 2D $MoTe_2$, the direct the phase transition from 2 H to T_d was also achieved by annealing. In order to avoid $MoTe_2$ evaporating at high vacuum and high annealing temperature, they used upper and lower 2 pieces of h-BN flakes for encapsulating [93]. By high annealing temperatures, single-crystal 2 H-$MoTe_2$ exhibits a anomalous dimensionality-driven phase transition to polycrystalline T_d-$MoTe_2$ with a 60° tilt-angle difference in all the grains (figure 3(f)). They tested the phase transition temperatures for samples with 1–7 layers and plotted a phase diagram of the annealing temperature (T_A) and the number of layers. The phase transition is dimensionality-dependent, and thinner 2 H-$MoTe_2$ performs a higher transition temperature. If T_A is higher than the phase transition temperature of thin $MoTe_2$ and lower than the phase transition temperature of thick $MoTe_2$, the phase transition occurs only in the thick region. Based on this principle, they can control the phase transition region, as well as prepare the 2 H–T_d hetero-phase junction.

Twisted-angle-induced transition. Creating symmetry breaking in non-ferroelectric parent compounds is crucial to obtain spontaneous polarization and ferroelectricity. Since the discovery of magic-angle graphene and other 2D superlattices, the twisted-angle gives an excellent opportunity to engineering symmetry in 2D materials [74, 105]. Graphene and h-BN are non-polar crystals with a centrosymmetric vdW structure. By introducing a moiré superlattice potential, Zheng *et al* discovered the switchable ferroelectricity in sandwich structural hBN/BLG layers, realizing the twisted-angle-induced transition from PE to FE [75]. In 2021, Shalom *et al* and Herrero *et al* reported that they could turn the intrinsic centrosymmetric h-BN into ferroelectric [65–67]. Bulk h-BN exhibits AA′ stacking and centrosymmetric. However, the AB or BA stacking can break the inversion symmetry, and trigger the distortion of the N–$2p_z$ orbital, which can create an OOP electric dipole (–P and +P) [106]. After applying a magic-angle twist between the h-BN sheets, large AA regions separated by AB and BA domains with distinct polarizations can be obtained (figure 3(g)). In Shalom's paper [66], the authors design two stacking modes: twisted angle of 0.5° and untwisted. In the twisted structure, this small twist exerts an evolving interlayer translation, creating a moiré pattern. In this case, there is a redistribution of charge between the h-BN layers, leading to polarization and ferroelectricity. For the untwisted mode, the authors introduce a displacement at the interface between the h-BN flakes, which can induce the interfacial polarization below.

Interfacial-polarization-induced transition. In addition to the ferroelectricity induced by twisted-angle, the interfacial polarization in multiple layers is also a cause of ferroelectricity. The interfacial ferroelectricity can be produced at the interface between two h-BN flakes, which are stacked with no twist [67]. As shown in figure 3(h), the top layer is switched between parallel and antiparallel stacking orientations, and the vertical charge redistributions cause interfacial net polarization (P_z). The introduced interfacial sliding or displacement with thickness of an odd number of layers at the interface between the flakes ensures antiparallel stacking (AA′, AB1′, or AB2′) on one side and parallel stacking (AA, AB, or BA) on the other side. This structure will trigger a redistribution of charge, which results in polarization and ferroelectricity. Moreover, the interfacial charge transfer by interlayer sliding also leads to the spontaneous polarization in 3 R MoS_2 and the yttrium-doped γ-InSe [50, 57]. Specifically, *P*. Meng *et al* found the anomalous intermediate polarization states in 3 R MoS_2 layers, and they proposed that layer number and interlayer dipole coupling play important roles in interfacial ferroelectricity. In another native centrosymmetric 2D material GaSe, its ferroelectricity stems from the intralayer sliding of the Se atomic layers, which breaks the mirror symmetry of local structures [52].

Stacking/heteroepitaxy-induced transition. Except for the twisted-angle-induced and interfacial-polarization-induced ferroelectricity, the stacking or heteroepitaxy growth without twisted-angle can also create ferroelectricity. In 2022, we reported the OOP ferroelectric and piezoelectric in untwisted, CVD-grown MoS_2/WS_2 heterobilayers (figure 3(i)) [70]. The MoS_2/WS_2 heterobilayers show a large d_{33}

piezoelectric constants of 1.95–2.09 pm V^{-1}, higher than In_2Se_3. By combining theoretical and experimental results, the ferroelectricity of MoS_2/WS_2 heterostructures is suggested to originate from the symmetry breaking and interlayer sliding. Additionally, in the stacked BP/WSe_2 heterostructures, in-plane electronic polarization and spontaneous photovoltaic effect have also been found [66]. The examples discussed above demonstrate that vdWs stacking or heteroepitaxy without twisted angles can effectively create extrinsic polarization.

Gaining a clear understanding of the thermodynamics and kinetics involved in phase transitions of 2D ferroelectrics is crucial for controlling crystalline phases and uncovering new phases. In the subsequent discussion, we will delve into several common mechanisms of 2D ferroelectrics, providing detailed insights into these aspects.

5. More features of phase transition in 2D ferroelectrics

Small energy differences. In general, when there are small energy differences between different phases, phase changes occur more easily. One of the most well-known examples of this is observed in monolayers of 2D molybdenum (Mo)- and tungsten (W)-based dichalcogenides (MoX_2, WX_2, where X = S, Se, Te). Every MoX_2 or WX_2 monolayer may have several stable and/or metastable phases (semiconducting 2 H, metallic 1 T and 1 T′). The DFT calculated ground-state energy differences of MoX_2 or WX_2 monolayers without strain are shown in figure 4(a), which reveals that the energy difference between the different phases is relatively small, especially 2 H and 1 T′ $MoTe_2$ (43 meV, figure 4(b)) [33]. Therefore, $MoTe_2$ is the most studied 2D phase-change material, and the phase transition between 2 H and 1 T′ can be achieved by a variety of ways, such as temperature, laser, electric-field, defect, strain, etc (figure 3). The kinetic study conducted on the phase transition of MoTe2 reveals that the transition from the 2 H phase to the 1 T′ phase is observable within a specific time frame of 50 s. Regarding the kinetic pathway of ferroelectric transition, an atypical case is the layered $CuInP_2S_6$ (CIPS) with quadruple-well potential property, which induces its ferroelectricity, negative piezoelectricity, and ionic conductivity [46]. The calculated change-in-energy curve plotted as polarization including high-polarization (±HP) and low-polarization (±LP) states is depicted in figure 4(c). The energy differences between ±HP and ±LP states are very small, and the switching between different polarization states is relatively easy by temperature, pressure, and bias. The Cu atom can be electrically displaced from its equilibrium Cu1 position into the vdW gap, which has a second stable position. This displacement causes the CIPS to change from a structure with two low-polarization minima to one with two additional high-polarization minima. We believe the existence of multiple well minima with polarization is a common occurrence in 2D vdW ferroelectrics.

Thermodynamic stability. Entropy is a broad quantity, so a reduction in dimension from 3D to 2D can result in a large reduction in latent heat. Thus, in most cases, much less energy is required to induce readable phase transitions in 2D materials compared to 3D materials. β'-In_2Se_3 was first discovered in 1975, but its phase transition to α-phase was never discovered. 2D β'-In_2Se_3 is thermodynamically metastable phase since the discovery of strain-induced phase [43]. The stable CVD growth of β'-In_2Se_3 films on mica is possible because the film is tightly attached to the atomically flat mica surface and its strain maintains this structure. Once the film is removed from the flat substrate and transferred to an uneven substrate, it will spontaneously transition to the thermodynamically stable α-phase (figure 4(d)). For example, we predeposit an array of gold particles on the SiO_2/Si substrate, and then transfer the β'-In_2Se_3 to the interface between the gold array and the SiO_2/Si substrate (figure 4(e)). On the uneven gold array, the metastable β'-In_2Se_3 film spontaneously undergoes a phase transition into the stable α-In_2Se_3. However, on the flat SiO_2/Si substrate, the film still maintains the original β'-phase. Finally, an in-plane β'-α heterophase junction is fabricated.

Recently proposed unconventional forms of ferroelectricity, including twisted ferroelectricity, moiré ferroelectricity, interfacial ferroelectricity, stacking ferroelectricity, and sliding ferroelectricity, have opened new possibilities in the realm of 2D vdW ferroelectricity. These unconventional ferroelectric phenomena mainly emerge because of structural phase transitions and interfacial charge transfers. Broadly speaking, they can be categorized into two main groups: moiré ferroelectricity and sliding ferroelectricity.

Moiré ferroelectricity. The 2D moiré superlattices provide a powerful platform for introducing new electronic structures and new physical phenomena. Moiré ferroelectricity can be produced by a small-angle-twisted stacking of two layers. Before moire ferroelectricity came out, it was difficult to imagine that centrosymmetric semi-metallic graphene could exhibit ferroelectricity. By using Bernal-stacked bilayer graphene within two h-BN layers (hBN/BLG/hBN), the unconventional moiré ferroelectricity was first realized [75]. The Bernal-stacked bilayer graphene itself is non-ferroelectricity. However, When the h-BN layers encapsulate the graphene, the moiré superlattice potential and symmetry breaking are produced. Similar moiré ferroelectricity cases are also found in twisted h-BN layers (figure 5(a)). Bulk h-BN is AA′ stacking with non-ferroelectricity, and the AA stacking is not stable. AB

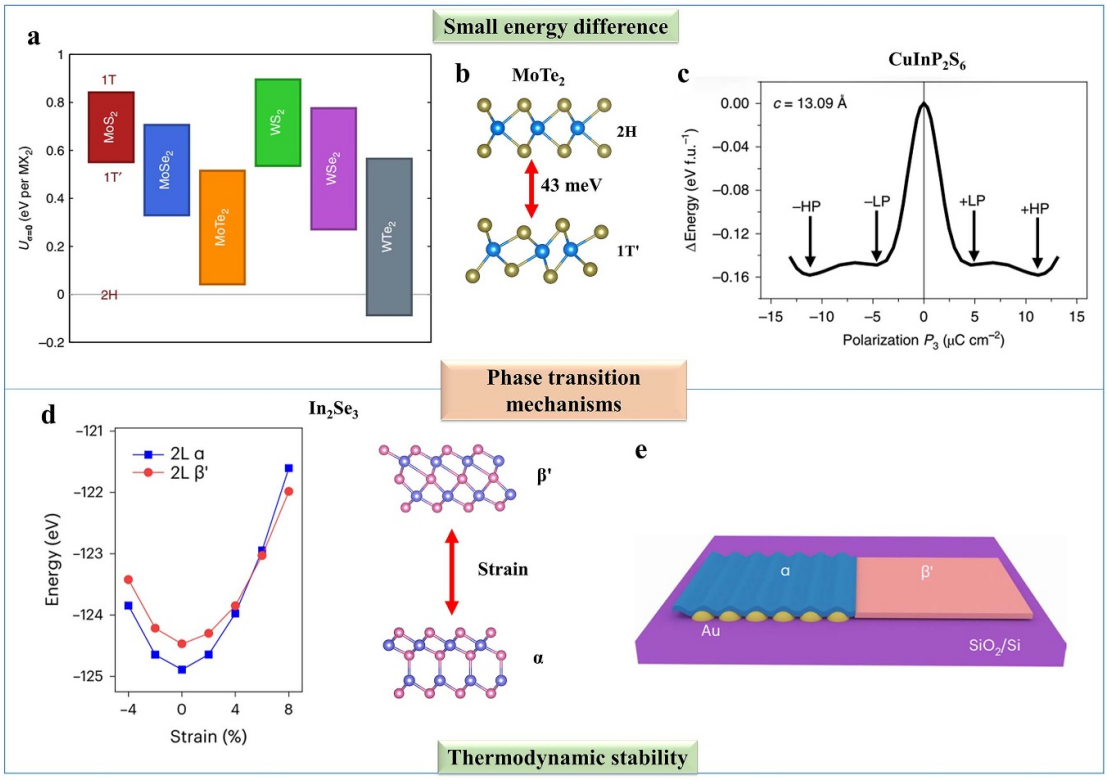

Figure 4. Phase transition mechanisms of 2D vdW ferroelectrics. (a) Ground-state energy differences among monolayer MoS_2, $MoSe_2$, $MoTe_2$, WS_2, WSe_2, and WTe_2. (b) The small energy differences (43 meV) between 1 T′ and 2 H $MoTe_2$. (c) Calculated change-in-energy curve plotted as polarization including high-polarization (±HP) and low-polarization (±LP) states. (d) Predicted total energy curves plotted as strain for bilayer β'-In_2Se_3 and α-In_2Se_3 flakes. e, Sketch diagram of strain-induced transition of β'-In_2Se_3 by Au-particle array. Panel (a) Reproduced from [33], with permission from Springer Nature. Panel (c) Reproduced from [46], with permission from Springer Nature. Panel (d) and (e) Reproduced from [43], with permission from Springer Nature.

or BA stacking is stable and polarized (figure 5(b)) [65, 66]. As depicted of left panel in figure 5(a), the small-angle twisted h-BN bilayer can form large AA areas separated by AB and BA domains. After atomic relaxation (right panel in figure 5(a)), this moiré pattern of alternating polarization AB and BA domains makes h-BN possessing moiré ferroelectricity [67]. Furthermore, twisted bilayer h-BN can act as a substrate that provides electrostatic moiré potential (V) for other functional layers [107]. As shown in figure 5(b), different stacking configurations produce different charge redistributions. Using moiré potential, twisted bilayer h-BN can regulate the electronic bands of functional layer, such as inhibit the exciton diffusion in $MoSe_2$. Therefore, electrostatic moiré potential (V) can be used to characterize the electric polarization generated by moiré ferroelectricity.

Sliding ferroelectricity. Different from the moiré ferroelectricity, the sliding ferroelectricity is realized via interlayer or lateral translation by about one bond length or untwisted stacking of bilayers. As depicted in figures 5(c) and (a) typical example is the distorted T-phase 2L-$MoTe_2$, where sliding between layers (a + b) is similar to mirror operation along the horizontal axis, resulting in the non-centrosymmetric degenerate ground states and OOP switching of polarization [68]. This ferroelectricity of bilayer T_d-$MoTe_2$ stems from interlayer sliding. The emergent OOP ferroelectricity in CVD-grown untwisted MoS_2/WS_2 heterobilayer is also attributed to symmetry breaking and interlayer sliding (figure 5(d)). The interfacial charge density difference of 3R-stacking MoS_2/WS_2 indicates the interfacial charge transfer and redistribution between the upper and lower layers [70]. The OOP polarization found in R-stacking bilayer WSe_2, $MoSe_2$, WS_2 and MoS_2 can be switched by an in-plane sliding motion. The meseared ferroelectric built-in interlayer potentials reveal that the charge redistribution causes the polarized electric field between layers. If a larger twisted-angle is used in a moiré bilayers, the interlayer strain will be introduced. This is the biggest difference between moiré ferroelectricity and sliding ferroelectricity. For example, in the strain field study in twisted-bilayer-graphene shows that (the twisted-angle is less than 2°), when the twisted-angle is applied to 1.23°, the interlayer strain is about 0.22%,

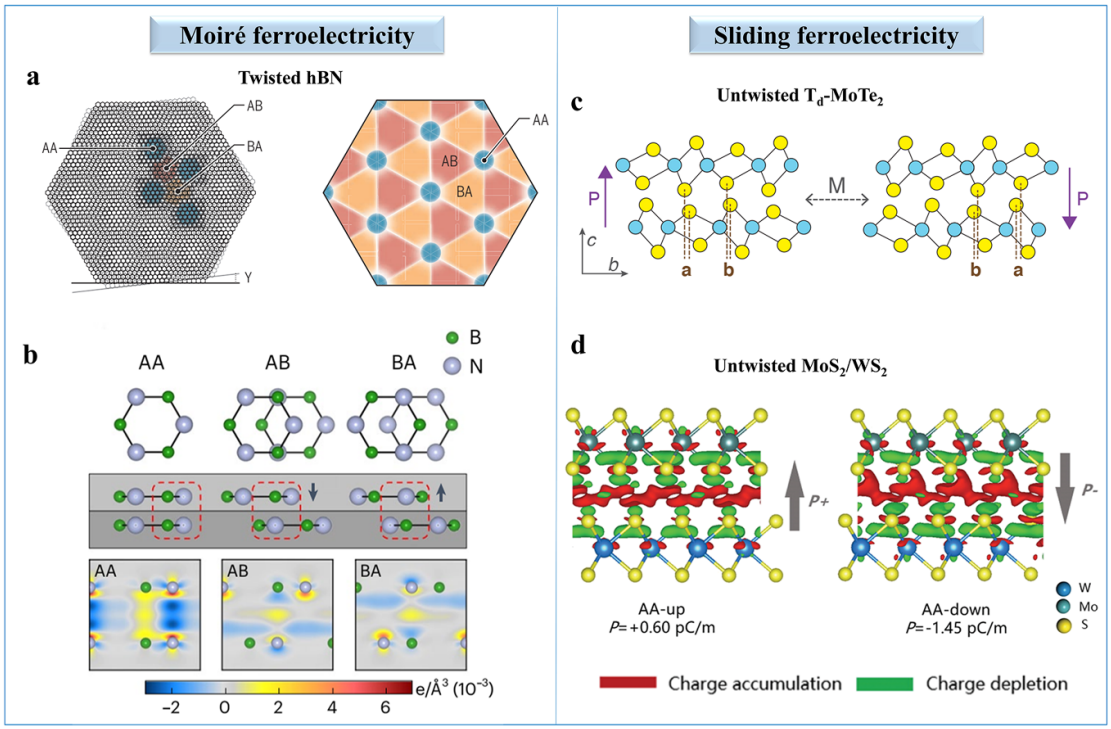

Figure 5. Comparison of the moiré ferroelectricity and the sliding ferroelectrics. (a) Structural sketches of the small-angle twisted bilayer h-BN and the calculated local-registry index (LRI) map after atomic relaxation. (b) Top and side views of the hBN parallel interface of AA, AB, and BA stacking structures. Down panel, the corresponding calculated charge redistribution. (c) Cross-sectional depiction of two stacked few-layered flakes of grown h-BN (AA') without twisting. (d) Interlayer differential charge density for the polarization up and down, respectively. Panel (a) adapted with permission from [67], AAAS. Panel (b) adapted from [107], Springer Nature Limited. Panel c adapted from [68], Springer Nature Limited. Panel (d) adapted from [70], AAAS. From [67]. Reprinted with permission from AAAS. Reproduced from [107], with permission from Springer Nature. Reproduced from [68], with permission from Springer Nature. From [70]. Reprinted with permission from AAAS.

greater than that of 0.16° [108]. It indicates that a relatively larger twisted-angle will bring about a larger interlayer strain in the moiré bilayers. This is not the case in sliding ferroelectricity.

6. *In situ* techniques for 2D ferroelectrics

In situ techniques provide the best means of studying the mechanism of phase transitions in real-time. In this regard, *in situ* TEM, *in situ* PFM, *in situ* Raman, *in situ* SHG and *in situ* Back-scattered electron channeling contrast imaging (BSECCI) are particularly useful.

***In situ* TEM**. By constructing different reactors or micro/nano devices in TEM holders, it can provide different external fields, such as heat, electrons, light, strain, and electrical bias, which can excite the phase transitions of 2D ferroelectrics. It makes *in situ* TEM a powerful tool to probe the structural phase transitions of 2D ferroelectrics from the nanoscale to atomic scale in real time. These structures include ferroelectric polar domains, electric-field distribution, and atomic structures [109]. At the same time, we can also understand how structure affects their properties and functions. Recently, we provided a comprehensive phase transition study of 2D In_2Se_3 by *In situ* TEM, including the β-InSe $\rightarrow$ β'-In_2Se_3 transition by heating, the $\beta' \leftrightarrow \alpha$ transition on In_2Se_3 film by strain (figure S1(a)), the $\alpha \rightarrow \beta' \rightarrow \gamma$ and $\alpha \rightarrow \gamma$ transition by electrical [43, 44].

***In situ* Raman**. The Raman effect originates from the inelastic scattering of materials to laser photons. Raman spectroscopy is useful for fingerprinting the structural information of materials, which is associated with the vibrational modes of lattices with Raman activity. Thus, all factors that can influence the vibrational modes of lattices, such as the temperature, electrostatic, electric-field, voltage bias, strain and chemical state, can affect the Raman spectrum [110]. In turn, we can also use the changes in Raman spectra to study the structural change in real-time in 2D materials. For 2D ferroelectrics, *in situ* Raman is an effective method to investigate their structural phase transitions (figure S1(b)) [40].

***In situ* SHG**. Second-harmonic-generation (SHG) is a nonlinear optical effect and can produce the frequency doubling of light. Noncentrosymmetry is the primary requirement for an SHG process due to the zero SHG coefficient ($\chi^2 = 0$) in all centrosymmetric structures [111]. A ferroelectric crystal is noncentrosymmetrical and can be identified by SHG. By

applying different external stimuli in real-time, *in situ* SHG becomes a non-destructive technique to observe the symmetry change of 2D ferroelectrics and it can determine the Curie temperature (T_c). Recently, Wan *et al* measured the ferroelectric transition temperature in 1 T′-ReS_2 multilayers by *in situ* heating SHG (figure S1(c)) [51].

***In situ* PFM**. The basic principle of PFM is to utilize the inverse-piezoelectric effect: the AC field is applied to the material surface by the AFM probe, resulting in surface deformation of the material. PFM has been widely used to characterize the piezoelectric and ferroelectric materials, including the piezoelectric coefficient, the ferroelectric domain imaging and domain switching behaviors [112]. *In situ* PFM operating in various fields can be used to observe the changes of ferroelectric properties in real-time. Recently, Guan *et al* reported a reversible AFE to FE phase transition at RT in 2D GeSe triggered by an external in-plane electric field (figure S1(d)) [95].

***In situ* BSECCI**. BSECCI is an imaging technique in the SEM that exploits the channeling effect of back-scattered electrons with respect to crystal lattice planes [113]. In 2D twisted bilayers, BSECCI can also provide a clear contrast and hence becomes a powerful tool to visualize the domain structure in 2D ferroelectrics. Using BSECCI, researchers can observe the subtle changes in the ferroelectric domain and domain walls (DWs). By applying an external electric field, we can adopt *in situ* BSECCI to observe the real-time change of ferroelectric domains with clear contrast. Recently, Weston *et al* used *in situ* BSECCI to investigate the evolution of triangular domain networks by applying an electric field (figure S1(e)) [78].

7. Multiferroic and superconducting phases in 2D ferroelectrics

In addition to ferroelectricity, 2D ferroelectrics can exhibit other interesting properties, like multiferroicity (antiferroelectricity, ferromagnetism, ferroelasticity) and superconductivity, etc.

AFE transition. Layered thiophosphates, with a formula of $CuInP_2X_6$ (X = S, Se), have emerged as 2D ferroelectric, ferrielectric or AFE. Ferrielectricity, the equivalent of ferrimagnetism, can be considered as AFE order but with a switchable polarization. Recently, Song *et al* presented that $CuInP_2Se_6$ possessed AFE ground state and ferrielectric- AFE transition in a thickness of 6–8 layers [114]. Afterward, Dziaugys *et al* reported the formation of a partially polarized AFE state and ferrielectric domains surrounded by the corresponding phase boundaries through quantitative imaging of nanoscale piezoelectric properties, as depicted in figure S2(a) [115]. The possible coexistence of ferrielectric and AFE states are evidenced by optical spectroscopies, Raman spectroscopy and DFT calculations. Moreover, they can manipulate the ferrielectric/ AFE phase transition by the electric field on the nanoscale, showing a new functionality in 2D ferroelectrics. For 2D β'-In_2Se_3, it was first reported as 2D ferroelectric, [116] but subsequent research suggests that it is more closely related to 2D AFE [117]. Xu *et al* revealed the in-plane antiferroelectricity in 2D β'-In_2Se_3 by optical and atomic scale electron microscopy with first-principles calculations. 2D β'-In_2Se_3 exhibits an unconventional nanostripe ordering, where individual nanostripes exhibit local ferroelectric polarization, while adjacent nanostripes are antipolar, resulting in a net polarization of zero. This AFE transition through the ordering of the superstructure is an intriguing phenomenon in 2D ferroelectrics.

Ferroelastic transition. As a type of ferroic property, ferroelasticity indicates the switchable spontaneous lattice strain by mechanical excitation. In 2021, Xu *et al* demonstrated the ferroelasticity in 2D AFE β'-In_2Se_3 flakes with few-layer thickness, as shown in figure S2(b) [118]. The 2D spontaneous strain stems from the in-plane AFE distortion evidenced by both atomic TEM and *in situ* x-ray diffraction. The equivalent strain orientations lead to three ferroelastic domain variants isolated by 60° and 120° DWs. The detailed domain switching mechanism is uncovered by *in situ* optical microscopy test on PET. Ferroelasticity switching between ferroelastic domains can be achieved with an external strain of $\leqslant$0.5%, demonstrating the potential for regulating the AFE polar structure and DW patterns through mechanical excitation. The discovery of 2D ferroelasticity in 2D ferroelectrics may lead to the development of novel memory and sensing devices.

Ferromagnetic transition. Due to the novel physical properties (magnetoelectric coupling, etc.) and multifunctional applications (memory device, spintronic device, etc), multiferroic materials with simultaneous ferromagnetic and ferroelectric orders have gained broad interest [63, 119]. Recently, Du *et al* reported a 2D multiferroic material of metallic p-doped SnSe with the coexistence of ferrimagnetism and ferroelectricity (figure S2(c)) [120]. The metallic feature in 2D p-doped SnSe arises from the local mixed phase of $SnSe_2$ microdomains and subsequent interfacial charge transfer. 2D p-doped SnSe shows a RT ferrimagnetism with a T_c of 337 K. The DFT calculations revealed that the asymmetric DOS of two spin channels gives rise to a total magnetic moment of $\sim$0.7881 μ_B, much higher than that of intrinsic SnSe ($\sim$0.5175 μ_B), evidencing the existence of ferrimagnetism in SnSe flakes.

Superconductive transition. In addition to multiferroic phases, the superconducting phase transition

is also found in 2D ferroelectrics. Superconductivity is a phenomenon in which the resistance of materials changes to zero below transition temperatures. High electrical conductivity in superconductivity counteracts the electric polarization, so that superconductivity and ferroelectricity are generally mutually exclusive. Jindal *et al* recently reported the coupled ferroelectricity and superconductivity in bilayer T_d-$MoTe_2$, as depicted in figure S2(d) [68]. They observed a first-order superconductor-to-normal transition in bilayer $MoTe_2$ together with a ferroelectric transition driven by the electric field. In $MoTe_2$ devices, charge-carrier doping and electric polarization can be independently adjusted, allowing for switching of the electrical polarization by changing the external field, which transforms the superconductor into a normal metal. The strong coupling between superconductivity and ferroelectricity enables ferroelectric control of a superconductor, potentially leading to the development of quantum devices in the future [121].

8. Emerging applications of 2D ferroelectrics

Berry curvature memory. Berry curvature is a physical quantity that characterizes the topological local entanglement between a crystal's conduction and valence bands. In 2D quantum materials, the stacking order of vdW layers can change the crystal symmetry and the electronic properties, including Berry curvature and ferroelectricity. Recently, an electrically induced stacking transition for designing Berry curvature non-volatile memory in 2D ferroelectric T_d-WTe_2 was discovered [122]. They made a dual-gate device based on WTe_2 flakes encapsulated by two h-BN flakes, as depicted in figure 6(a). A small number of carriers are injected under a longitudinal electric field to the WTe_2 layers, allowing each odd layer to produce in-plane interlayer sliding. The considerable Berry curvature in WTe_2 layers is utilized to read data stored between these moving atomic layers. This quantum feature can distinguish stacking orders and metal polarization states, as different stacking orders exhibit distinct Berry curvatures. This finding addresses the long-standing challenge of reading the real-space weak polarity in 2D ferroelectric metals.

RRAM. 2H-$MoTe_2$ and 1T′-$MoTe_2$ phases are prone to generate phase transition by electrical stimulation due to their lowest energy difference in all TMDs. Because of the differences in resistance and ferroelectricity between 2H and 1T′ or T_d phases, the memory performance using this phase transition can be obtained by switching the resistive and polarization states. In 2019, Appenzeller *et al* reported the electric-field-induced phase transition from 2H phase to $2H_d$ and T_d phases in the vertical 2H-$MoTe_2$ and $Mo_{1-x}W_xTe_2$-based RRAM devices, as shown in figure 6(b) [102]. Unlike traditional RRAM devices, $MoTe_2$ exhibits conductive filaments and new crystal structures, including a previously unidentified $2H_d$ phase, as revealed in the study. The structure of this phase differs from the well-known 2H, 1T′, and T_d phases, and can be used to regulate the high and low resistance states of the device by applying an electric field. The RRAM devices exhibit an ultrafast resistive switching speed of 10 ns and a high on/off current ratio of 10^6 with programming currents lower than 1 μA. This study suggests that controlled phase transitions can be achieved through electrical manipulation in 2D ferroelectrics, indicating their significant potential for use in memory devices.

Ferroelectric phase change transistor. In addition to applying an electric field to change the phase of 2D $MoTe_2$, its phase can also be altered by applying strain. A non-volatile $MoTe_2$ phase change transistor by strain engineering was shown in figure 6(c) [41]. $MoTe_2$ can be switched from 1T′ to 2H phase driven by electric-field-induced strain on ferroelectric $Pb(Mg_{1/3}Nb_{2/3})_{0.71}Ti_{0.29}O_3$ (PMN-PT) single-crystal substrate. Compared to the normal on/off ratio limitation of field-effect transistors, the $MoTe_2$ phase-change transistor can achieve an ultrahigh on/off ratio because the 'on' state of this device is fully metallic, resulting in a high current. Additionally, contact engineering can significantly reduce the 'off' state current, enabling large non-volatile changes in channel conductivity. This strain-driven, non-volatile phase-change transistor demonstrates the potential of 2D materials in the development of superfast (sub-nanosecond) and low-power consumption (attojoule) logic and memory devices.

Hetero-phase junction ferroelectric transistor. Phase change engineering of 2D ferroelectrics can usually fabricate the in-plane homojunctions or hetero-phase junctions, such as 2H-1T MoS_2, 2H-1T′ $MoTe_2$, etc. For instance, by utilizing the strain-driven phase transition of In_2Se_3, we have prepared an in-plane α–β' hetero-phase junction ferroelectric transistor with a ferroelectric- AFE configuration, which exhibits outstanding non-volatile memory performance, as demonstrated in figure 6(d) [43]. Encouraged by the strain-release induced phase transition, we used e-beam evaporated Au pattern as a rough surface and SiO_2/Si substrate as a flat surface to fabricate an α–β' hetero-phase junction by one-step transfer. After transfer onto the Au pattern, the pristine β'-phase In_2Se_3 film transforms into α-phase in the uneven Au pattern area owing to the release of in-plane strain, while the area on the flat SiO_2/Si substrates remains intact, maintaining the pristine β' phase. Some wrinkles appear in the α-phase area, a signature of film delamination and β'–α phase transition. The Raman mapping result shows that the two-phase merged area is uniform, and the interface

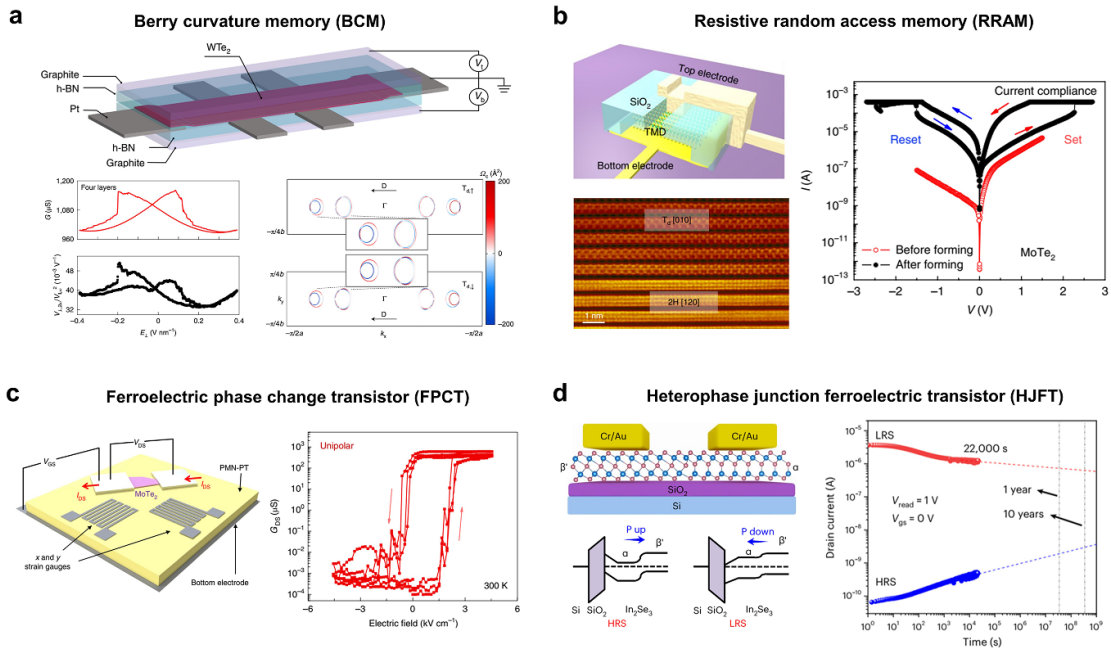

Figure 6. Emerging device applications of 2D ferroelectrics with additional phase control. (a) Upper panel, schematic of dual-gate WTe_2 memory device. Lower panel, electric-field-driven longitudinal conductance (upper left) and nonlinear Hall signal (lower left) in WTe_2, and the corresponding calculated Berry curvature in the 2D Brillouin zone at the Fermi level (right). (b) Left panel, schematic of a vertical $MoTe_2$ device, and atomic HAADF image of T_d phase and 2 H phase. Right panel, *I–V* curves of a vertical $MoTe_2$ device. (c) Left panel, schematic of the $MoTe_2$ ferroelectric strain device. Right panel, three full *G–E* loops of the unipolar $MoTe_2$ device. (d) Left panel, schematic of the FET device (above) and the corresponding band diagram (below) of α–β' junction. Right panel, NVM retention performance of the α–β' junction device by gate-voltage write and erase. Panel (a) Reproduced from [122], with permission from Springer Nature. Panel (b) Reproduced from [102], with permission from Springer Nature. Panel (c) Reproduced from [41], with permission from Springer Nature. Panel (d) Reproduced from [43], with permission from Springer Nature.

is sharp and seamless. The α–β' junction benefits from the built-in field and the degree of freedom in polarization control under an external electric field, and its device shows a wider hysteresis window (43.8 V under—40.0–40.0 V sweeping) and greater non-volatile memory performance (retention time of 22 000 s and endurance for 6000 cycles) than that of the single-phase devices.

9. Challenges and outlook

Despite the discovery of some phase transition mechanisms in 2D ferroelectrics in recent years, their research and development still face numerous challenges. Firstly, the phase transition mechanisms between ferroelectric and non-ferroelectric phases of most intrinsic 2D ferroelectric materials are poorly understood. Additionally, the mechanism for transforming non-ferroelectric materials into extrinsic ferroelectricity is still in its early stages of research. In future research, we suggest focusing on several key areas:

Exploring and creating new 2D ferroelectrics. The first task is to discover new intrinsic 2D ferroelectric materials and investigate their phase transition mechanisms using both *in situ* and ex situ approaches. Currently, only 23 types of intrinsic 2D ferroelectric materials have been experimentally validated, and the development rate lags behind that of intrinsic 2D magnetic materials (which were discovered in 2017, and now over 50 have been confirmed) [123, 124]. Searching for new 2D ferroelectric materials is extremely important for the basic physical research and future device applications. However, due to the weak polarization intensity of 2D ferroelectrics, it is difficult to be applied in electronic devices at the current stage. How to improve the polarization intensity of current 2D ferroelectric materials and find new materials with strong polarization are two urgent research directions. In order to improve the efficiency of research, we can use artificial intelligence (AI) to explore ways to improve the polarization intensity of current 2D ferroelectric materials, such as doping, modification and so on. At the same time, we can also use AI to predict new 2D ferroelectric materials with strong polarization.

Besides, first-principles calculations can help us to find new intrinsic 2D ferroelectrics. For instance, monolayer monochalcogenides MX (M = Ge, Sn; X = S, Se) were predicted to show spontaneous in-plane electrical polarization and ferroelectricity in 2016, however, GeS has not yet been proven to be ferroelectric [36]. Other materials like GaS, GaTe, VOI_2, VS_2, Bi_2O_2S, Bi_2O_2Te, etc. have also shown

promising potential for room-temperature ferroelectricity in theoretical studies [8, 125, 126]. SHG and PFM are valuable tools for identifying ferroelectric materials and measuring their Curie temperatures. In addition, in situ/ex situ TEM and Raman spectroscopy can be used to probe their phase transition mechanisms, including thermodynamics and kinetics, under various external stimuli. The BSECCI technique can reveal the evolution of DWs under an electric field.

Understanding phase transitions mechanisms and domain dynamics. Understanding the novel ferroelectric orders down to the atomic scale are important in the various emerging 2D ferroelectric phases including intrinsic ferroelectrics and extrinsic ferroelectrics, such as those induced by twisted-angle, stacking-order, and heteroepitaxy. By uncovering the underlying physics of these mechanisms, we can develop new strategies for manipulating and optimizing the ferroelectric properties of 2D materials. This knowledge is essential for the development of next-generation electronics, energy harvesting, and sensing devices that rely on the unique properties of ferroelectric materials [127]. For non-vdW ferroelectric films, such as $BiFeO_3$ and $Pb(Zr_{0.2}Ti_{0.8})O_3$ (PZT), researchers have studied their kinetics and dynamics of ferroelectric switching at atomic resolution by aberration-corrected transmission electron microscopy [128, 129]. However, for 2D ferroelectrics including In_2Se_3, research on the atomic mechanisms of ferroelectric switching is still limited. Therefore, a key future task is to investigate the atomic-level mechanisms of 2D ferroelectricity using state-of-the-art techniques, including 4D-STEM, differential-phase-contrast, and momentum-resolved EELS (q-EELS) [130]. Additionally, machine learning algorithms can be used to process TEM data and provide quantitative results.

Creating new extrinsic ferroelectrics. Through various methods such as twisting, stacking, or heteroepitaxy-based phase engineering, non-ferroelectric 2D materials can be transformed into ferroelectric materials, significantly expanding the pool of available ferroelectric materials. Additionally, new approaches must be developed to create extrinsic ferroelectrics from non-ferroelectric 2D building blocks. For instance, β-In_2Se_3 and black phosphorus (BP) are non-ferroelectric vdW layered materials, which may transition to 2D ferroelectrics by stacking two layers with a small twisting angle. Moreover, constructing vertical or transverse heterojunctions with ferroelectric materials can break symmetry and induce polar DWs [32]. In addition, strain engineering is an effective method to break the C_3 rotational symmetry, such as in a bended MoS_2 device [131]. Meanwhile, the C_3 rotational symmetry breaking can trigger the structural phase transition as well. Other methods for phase control and symmetry breaking include molecule intercalation, [24] atom doping, [132] and electron-beam irradiation [133].

Wafer-scale growth. Large-scale commercial applications of 2D ferroelectrics require the growth of wafer-scale single-crystal thin films with uniformity and low-cost [134]. However, most samples are limited to the micrometer scale, with only a few reaching centimeter-size. However, a recent low-thermal-budget growth method (growth temperature $< 300\,^{\circ}C$) for monolayer 8 inch MoS_2 films has been reported, which is a silicon complementary metal–oxide–semiconductor compatible route and can be integrated in the BEOL process [135]. This method could provide inspiration for growing large-area 2D ferroelectric materials through MOCVD at a low growth temperature.

Discover multiferroicity and their coupling effect. 2D multiferroic vdW materials with both ferroelectric and ferromagnetic (antiferromagnetic) properties have been the focus of research in recent years, including NiI_2, [62] $CuCrP_2S_6$, [63] p-doped SnSe, [120] and Fe-doped In_2Se_3 [136]. Because the magnetoelectric coupling effect can realize the control of magnetic field, 2D multiferroic vdW materials have potential applications in spin-ferroelectric transistors and magnetic memory. In addition to looking for intrinsic 2D multiferroic materials, we can artificially create multiferroicity. Another approach involves creating 2D ferromagnetic materials with inherent ferroelectricity by twisting and stacking two layers of such materials. Investigating the response of 2D multiferroic vdW materials to external stimuli like light and strain is also an area of interest. Understanding the optical-ferroelectric-ferromagnetic coupling effect in these materials, holds promise for the development of multifunctional devices.

Constructing novel ferroelectric-based devices. Compared to traditional 3D ferroelectric materials, 2D ferroelectrics offer significant advantages, including their atomic-scale thickness and the flexibility of stacking engineering, akin to 'LEGO' blocks. This stacking flexibility allows us to not only utilize the properties of individual 2D materials but also leverage the coupling properties of their heterojunctions. One current disadvantage of 2D ferroelectrics is their relatively small OOP polarization value, one order of magnitude lower than that of traditional ferroelectrics such as HfO_2, PVDF and $Pb(Zr,Ti)O_3$ [137]. Hence, using strong polarization materials as dielectric, substrate, or intermediate layer can greatly improve the polarization intensity and memory performance of the 2D–3D hybrid devices [138]. In addition, constructing a ferroelectric-ferromagnetic-based multiferroic heterojunction device using a 2D or 3D ferromagnetic material shows promise for

magnetic memories and spin transistors, due to the magnetoelectric coupling effect [139]. Furthermore, utilizing the structural and ferroelectric phase transitions of 2D ferroelectrics to construct memory devices is a new trend for future developments in this field.

Memristor with crossbar structure is one of the main structures of the commercial memory. They can form neural networks through large-scale crossbar arrays to conduct parallel and efficient in-memory computing [140]. In 2D vdW ferroelectrics, ferroelectric and structural phase transitions can be used as memristor switching mechanisms. Such memristors can be controlled by electric-field or strain, such as the recently reported $MoTe_2$ phase-change memristor and phase-change memtransistive synapses [141, 142]. Furthermore, there is a need for further exploration into the operational mechanisms of 2D ferroelectric memristors [143, 144]. Understanding how to achieve phase-change memristors and enhance their performance requires significant research and development. There is still a substantial amount of work awaiting us in this area [144, 145].

We strongly believe that the phase engineering in 2D vdW ferroelectrics is a promising area for future physics and materials research, with the potential to yield novel physical properties, new phase transition mechanisms, new 2D vdW ferroelectrics, innovative preparation methods, and advanced electronic devices.

Data availability statement

All data that support the findings of this study are included within the article (and any supplementary files).

Acknowledgments

This work was supported by National Natural Science Foundation of China (Grant Nos. 22105162, 52173230, 52222218, 52272045), the Hong Kong Research Grant Council General Research Fund (Project Nos. 11312022, 15302522, 11300820, 15302419, 15301623, 15306321), The Innovation and Technology Fund (Project No. ITS/014/23), the Hong Kong Research Grant Council Collaborative Research Fund (Project No. C5067-23G), the City University of Hong Kong (Project Nos. 7006005, 9680241, 9678303), The Hong Kong Polytechnic University (Project Nos. SAC9), Environment and Conservation Fund (Project Nos. 34/2022), the Shenzhen Science, Technology and Innovation Commission (Project No. SGDX20230821092059005), Major Program (JD) of Hubei Province under Grant No. 2023BAA009, the Science and Technology Major Project of Hubei under Grant No. 2020AAA005, and the Science and Technology Major Project of Wuhan under Grant No. 2021012002023423.

Conflict of interest

The authors declare no competing interests.

Author contributions

J Z led the research project. W H and J Z wrote the manuscript with H W, S PL, J W, and T H L's assistance. All the authors discussed and approved the manuscript.

ORCID iDs

Wei Han https://orcid.org/0000-0001-9662-1415
Hao Wang https://orcid.org/0000-0002-4894-7653
Jiong Zhao https://orcid.org/0000-0002-7411-0734

References

[1] Valasek J 1921 Piezoelectric and allied phenomena in Rochelle salt *Phys. Rev.* **17** 475–81
[2] Cohen R E 1992 Origin of ferroelectricity in perovskite oxides *Nature* **358** 136–8
[3] Ji D *et al* 2019 Freestanding crystalline oxide perovskites down to the monolayer limit *Nature* **570** 87–90
[4] Bennett J W, Grinberg I and Rappe A M 2008 New highly polar semiconductor ferroelectrics through *d*8 cation-O vacancy substitution into $PbTiO_3$: a theoretical study *J. Am. Chem. Soc.* **130** 17409–12
[5] Wang Q H, Kalantar-Zadeh K, Kis A, Coleman J N and Strano M S 2012 Electronics and optoelectronics of two-dimensional transition metal dichalcogenides *Nat. Nanotechnol.* **7** 699–712
[6] Novoselov K S, Mishchenko A, Carvalho A and Castro Neto A H 2016 2D materials and van der Waals heterostructures *Science* **353** aac9439
[7] Liu Y, Duan X, Shin H-J, Park S, Huang Y and Duan X 2021 Promises and prospects of two-dimensional transistors *Nature* **591** 43–53
[8] Guan Z, Hu H, Shen X, Xiang P, Zhong N, Chu J and Duan C 2020 Recent progress in two-dimensional ferroelectric materials *Adv. Electron. Mater.* **6** 1900818
[9] Wu M 2021 Two-dimensional van der Waals ferroelectrics: scientific and technological opportunities *ACS Nano* **15** 9229–37
[10] Chang K *et al* 2016 Discovery of robust in-plane ferroelectricity in atomic-thick SnTe *Science* **353** 274–8
[11] Qi L, Ruan S and Zeng Y-J 2021 Review on recent developments in 2D ferroelectrics: theories and applications *Adv. Mater.* **33** 2005098
[12] Zhang D, Schoenherr P, Sharma P and Seidel J 2023 Ferroelectric order in van der Waals layered materials *Nat. Rev. Mater.* **8** 25–40
[13] Wang C, You L, Cobden D and Wang J 2023 Towards two-dimensional van der Waals ferroelectrics *Nat. Mater.* **22** 542–52
[14] Wang S, Liu L, Gan L, Chen H, Hou X, Ding Y, Ma S, Zhang D W and Zhou P 2021 Two-dimensional ferroelectric channel transistors integrating ultra-fast memory and neural computing *Nat. Commun.* **12** 53
[15] Wang X W *et al* 2021 Van der Waals engineering of ferroelectric heterostructures for long-retention memory *Nat. Commun.* **12** 1109
[16] Si M *et al* 2019 A ferroelectric semiconductor field-effect transistor *Nat. Electron.* **2** 580–6

[17] Khan A I, Keshavarzi A and Datta S 2020 The future of ferroelectric field-effect transistor technology *Nat. Electron.* **3** 588–97
[18] Ielmini D and Wong H-S P 2018 In-memory computing with resistive switching devices *Nat. Electron.* **1** 333–43
[19] Liu Y, Huang Y and Duan X 2019 Van der Waals integration before and beyond two-dimensional materials *Nature* **567** 323–33
[20] Yang Q, Wu M and Li J 2018 Origin of two-dimensional vertical ferroelectricity in WTe_2 bilayer and multilayer *J. Phys. Chem. Lett.* **9** 7160–4
[21] Sutter P, Komsa H P, Lu H, Gruverman A and Sutter E 2021 Few-layer tin sulfide (SnS): controlled synthesis, thickness dependent vibrational properties, and ferroelectricity *Nano Today* **37** 101082
[22] Hohenberg P C 1967 Existence of long-range order in one and two dimensions *Phys. Rev.* **158** 383–6
[23] Belianinov A, He Q, Dziaugys A, Maksymovych P, Eliseev E, Borisevich A, Morozovska A, Banys J, Vysochanskii Y and Kalinin S V 2015 $CuInP_2S_6$ room temperature layered ferroelectric *Nano Lett.* **15** 3808–14
[24] Wu M 2021 100 years of ferroelectricity *Nat. Rev. Phys.* **3** 726
[25] Dawber M, Rabe K and Scott J 2005 Physics of thin-film ferroelectric oxides *Rev. Mod. Phys.* **77** 1083–130
[26] Kim D J, Jo J Y, Kim Y S, Chang Y J, Lee J S, Yoon J-G, Song T K and Noh T W 2005 Polarization relaxation induced by a depolarization field in ultrathin ferroelectric $BaTiO_3$ capacitors *Phys. Rev. Lett.* **95** 237602
[27] Li W, Qian X and Li J 2021 Phase transitions in 2D materials *Nat. Rev. Mater.* **6** 829–46
[28] Yang H, Kim S W, Chhowalla M and Lee Y H 2017 Structural and quantum-state phase transitions in van der Waals layered materials *Nat. Phys.* **13** 931–7
[29] Chen Y, Lai Z, Zhang X, Fan Z, He Q, Tan C and Zhang H 2020 Phase engineering of nanomaterials *Nat. Rev. Chem.* **4** 243–56
[30] Wu Y, Li D, Wu C L, Hwang H Y and Cui Y 2023 Electrostatic gating and intercalation in 2D materials *Nat. Rev. Mater.* **8** 41–53
[31] Du L, Hasan T, Castellanos-Gomez A, Liu G-B, Yao Y, Lau C N and Sun Z 2021 Engineering symmetry breaking in 2D layered materials *Nat. Rev. Phys.* **3** 193–206
[32] Wang R, Yu Y, Zhou S, Li H, Wong H, Luo Z, Gan L and Zhai T 2018 Strategies on phase control in transition metal dichalcogenides *Adv. Funct. Mater.* **28** 1802473
[33] Duerloo K-A N, Li Y and Reed E J 2014 Structural phase transitions in two-dimensional Mo- and W-dichalcogenide monolayers *Nat. Commun.* **5** 4214
[34] Yin X M, Tang C S, Zheng Y, Gao J, Wu J, Zhang H, Chhowalla M, Chen W and Wee A T S 2021 Recent developments in 2D transition metal dichalcogenides: phase transition and applications of the (quasi-)metallic phases *Chem. Soc. Rev.* **50** 10087–115
[35] Huang Y-T, Chen N-K, Li Z-Z, Wang X-P, Sun H-B, Zhang S and Li X-B 2022 Two-dimensional In2Se3: a rising advanced material for ferroelectric data storage *InfoMat* **4** e12341
[36] Fei R, Kang W and Yang L 2016 Ferroelectricity and phase transitions in monolayer group-IV monochalcogenides *Phys. Rev. Lett.* **117** 097601
[37] Li D and Lu S-G 2018 Electrocaloric effect and phase transitions in ferroelectrics *Int J. Metall. Mater. Eng.* **4** 141
[38] Liu K, Lu J, Picozzi S, Bellaiche L and Xiang H 2018 Intrinsic origin of enhancement of ferroelectricity in SnTe ultrathin films *Phys. Rev. Lett.* **121** 027601
[39] Yuan S, Luo X, Chan H L, Xiao C, Dai Y, Xie M and Hao J 2019 Room-temperature ferroelectricity in $MoTe_2$ down to the atomic monolayer limit *Nat. Commun.* **10** 1775
[40] Wang Y *et al* 2017 Structural phase transition in monolayer $MoTe_2$ driven by electrostatic doping *Nature* **550** 487–91
[41] Hou W, Azizimanesh A, Sewaket A, Peña T, Watson C, Liu M, Askari H and Wu S M 2019 Strain-based room-temperature non-volatile $MoTe_2$ ferroelectric phase change transistor *Nat. Nanotechnol.* **14** 668–73
[42] Fei Z, Zhao W, Palomaki T A, Sun B, Miller M K, Zhao Z, Yan J, Xu X and Cobden D H 2018 Ferroelectric switching of a two-dimensional metal *Nature* **560** 336–9
[43] Han W *et al* 2023 Phase-controllable large-area two-dimensional In_2Se_3 and ferroelectric hetero-phase junction *Nat. Nanotechnol.* **18** 55–63
[44] Zheng X D *et al* 2022 Phase and polarization modulation in two-dimensional In_2Se_3 via *in situ* transmission electron microscopy *Sci. Adv.* **8** eabo0773
[45] Zhou Y *et al* 2017 Out-of-plane piezoelectricity and ferroelectricity in layered α-In_2Se_3 nanoflakes *Nano Lett.* **17** 5508–13
[46] Brehm J *et al* 2020 Tunable quadruple-well ferroelectric van der Waals crystals *Nat. Mater.* **19** 43–48
[47] Liu F *et al* 2016 Room-temperature ferroelectricity in $CuInP_2S_6$ ultrathin flakes *Nat. Commun.* **7** 12357
[48] Chang K, Küster F, Miller B J, Ji J-R, Zhang J-L, Sessi P, Barraza-Lopez S and Parkin S S P 2020 Microscopic manipulation of ferroelectric domains in SnSe monolayers at room temperature *Nano Lett.* **20** 6590–7
[49] Higashitarumizu N, Kawamoto H, Lee C-J, Lin B-H, Chu F-H, Yonemori I, Nishimura T, Wakabayashi K, Chang W-H and Nagashio K 2020 Purely in-plane ferroelectricity in monolayer SnS at room temperature *Nat. Commun.* **11** 2428
[50] Meng P *et al* 2022 Sliding induced multiple polarization states in two-dimensional ferroelectrics *Nat. Commun.* **13** 7696
[51] Wan Y *et al* 2022 Room-temperature ferroelectricity in 1T′-ReS_2 multilayers *Phys. Rev. Lett.* **128** 067601
[52] Li W *et al* 2023 Emergence of ferroelectricity in a nonferroelectric monolayer *Nat. Commun.* **14** 2757
[53] Xue W *et al* 2022 Discovery of robust ferroelectricity in 2D defective semiconductor α-Ga_2Se_3 *Small* **18** 2105599
[54] Ghosh T, Samanta M, Vasdev A, Dolui K, Ghatak J, Das T, Sheet G and Biswas K 2019 Ultrathin free-standing nanosheets of Bi_2O_2Se: room temperature ferroelectricity in self-assembled charged layered heterostructure *Nano Lett.* **19** 5703–9
[55] Xu X, Zhong T, Zuo N, Li Z, Li D, Pi L, Chen P, Wu M, Zhai T and Zhou X 2022 High-T_C two-dimensional ferroelectric $CuCrS_2$ grown via chemical vapor deposition *ACS Nano* **16** 8141–9
[56] Peng Q *et al* 2021 Room-temperature ferroelectricity in 2D metal–tellurium–oxyhalide $Cd_7Te_7Cl_8O_{17}$ via selenium-induced selective-bonding growth *ACS Nano* **15** 16525–32
[57] Sui F, Jin M, Zhang Y, Qi R, Wu Y-N, Huang R, Yue F and Chu J 2023 Sliding ferroelectricity in van der Waals layered γ-InSe semiconductor *Nat. Commun.* **14** 36
[58] You L *et al* 2018 In-plane ferroelectricity in thin flakes of van der Waals hybrid perovskite *Adv. Mater.* **30** 1803249
[59] Abdelwahab I *et al* 2022 Giant second-harmonic generation in ferroelectric $NbOI_2$ *Nat. Photon.* **16** 644–50
[60] Han M *et al* 2022 Continuously tunable ferroelectric domain width down to the single-atomic limit in bismuth tellurite *Nat. Commun.* **13** 5903
[61] Jeong K, Lee H, Lee C, Wook L H, Kim H, Lee E and Cho M-H 2021 Ferroelectric switching in GeTe through rotation of lone-pair electrons by electric field-driven phase transition *Appli. Mater. Today* **24** 101122
[62] Io W F *et al* 2023 Direct observation of intrinsic room-temperature ferroelectricity in 2D layered $CuCrP_2S_6$ *Nat. Commun.* **14** 7304
[63] Song Q *et al* 2022 Evidence for a single-layer van der Waals multiferroic *Nature* **602** 601–5
[64] Gou J, Bai H, Zhang X, Huang Y L, Duan S, Ariando A, Yang S A, Chen L, Lu Y and Wee A T S 2023 Two-dimensional ferroelectricity in a single-element bismuth monolayer *Nature* **617** 67–72

[65] Yasuda K, Wang X, Watanabe K, Taniguchi T and Jarillo-Herrero P 2021 Stacking-engineered ferroelectricity in bilayer boron nitride *Science* **372** 1458–62
[66] Vizner Stern M, Waschitz Y, Cao W, Nevo I, Watanabe K, Taniguchi T, Sela E, Urbakh M, Hod O and Ben Shalom M 2021 Interfacial ferroelectricity by van der Waals sliding *Science* **372** 1462–6
[67] Tsymbal E Y 2021 Two-dimensional ferroelectricity by design *Science* **372** 1389–90
[68] Jindal A *et al* 2023 Coupled ferroelectricity and superconductivity in bilayer T_d-$MoTe_2$ *Nature* **613** 48–52
[69] Cao Y, Fatemi V, Fang S, Watanabe K, Taniguchi T, Kaxiras E and Jarillo-Herrero P 2018 Unconventional superconductivity in magic-angle graphene superlattices *Nature* **556** 43–50
[70] Rogée L, Wang L, Zhang Y, Cai S, Wang P, Chhowalla M, Ji W and Lau S P 2022 Ferroelectricity in untwisted heterobilayers of transition metal dichalcogenides *Science* **376** 973–8
[71] Ding W J, Zhu J, Wang Z, Gao Y, Xiao D, Gu Y, Zhang Z and Zhu W 2017 Prediction of intrinsic two-dimensional ferroelectrics in In_2Se_3 and other III2-VI3 van der Waals materials *Nat. Commun.* **8** 14956
[72] Xue F *et al* 2018 Room-temperature ferroelectricity in hexagonally layered α-In_2Se_3 nanoflakes down to the monolayer limit *Adv. Funct. Mater.* **28** 1803738
[73] Cui C *et al* 2018 Intercorrelated in-plane and out-of-plane ferroelectricity in ultrathin two-dimensional layered semiconductor In_2Se_3 *Nano Lett.* **18** 1253–8
[74] Cao Y *et al* 2018 Correlated insulator behaviour at half-filling in magic-angle graphene superlattices *Nature* **556** 80–84
[75] Zheng Z *et al* 2020 Unconventional ferroelectricity in moiré heterostructures *Nature* **588** 71–76
[76] Deb S, Cao W, Raab N, Watanabe K, Taniguchi T, Goldstein M, Kronik L, Urbakh M, Hod O and Ben Shalom M 2022 Cumulative polarization in conductive interfacial ferroelectrics *Nature* **612** 465–9
[77] Wang X, Yasuda K, Zhang Y, Liu S, Watanabe K, Taniguchi T, Hone J, Fu L and Jarillo-Herrero P 2022 Interfacial ferroelectricity in rhombohedral-stacked bilayer transition metal dichalcogenides *Nat. Nanotechnol.* **17** 367–71
[78] Weston A *et al* 2022 Interfacial ferroelectricity in marginally twisted 2D semiconductors *Nat. Nanotechnol.* **17** 390–5
[79] Akamatsu T *et al* 2021 A van der Waals interface that creates in-plane polarization and a spontaneous photovoltaic effect *Science* **372** 68–72
[80] Kang K F, Zhao W, Zeng Y, Watanabe K, Taniguchi T, Shan J and Mak K F 2023 Switchable moiré potentials in ferroelectric WTe_2/WSe_2 superlattices *Nat. Nanotechnol.* **18** 861–6
[81] Wong L W *et al* 2024 Deciphering the ultra-high plasticity in metal monochalcogenides *Nat. Mater.* **23** 196–204
[82] Xia Y *et al* 2023 12-inch growth of uniform MoS_2 monolayer for integrated circuit manufacture *Nat. Mater.* **22** 1324–31
[83] Xu X L *et al* 2021 Seeded 2D epitaxy of large-area single-crystal films of the van der Waals semiconductor 2H $MoTe_2$ *Science* **372** 195–200
[84] Zhang Y, Wang Z, Feng J, Ming S, Qu F, Xia Y, He M, Hu Z and Wang J 2022 Synthesis and electromagnetic transport of large-area 2D WTe_2 thin film *J. Semicond.* **43** 102002
[85] Kwon K C *et al* 2020 In-plane ferroelectric tin monosulfide and its application in a ferroelectric analog synaptic device *ACS Nano* **14** 7628–38
[86] Jo H-K *et al* 2023 Wafer-scale production of two-dimensional tin monoselenide: expandable synthetic platform for van der Waals semiconductor-based broadband photodetectors *ACS Nano* **17** 1372–80
[87] Miao J and Murnane M M 2023 Epitaxial substitution of metal iodides for low-temperature growth of two-dimensional metal chalcogenides *Nat. Nanotechnol.* **18** 1–8
[88] Khan U, Nairan A, Khan K, Li S, Liu B and Gao J 2023 Salt-assisted low-temperature growth of 2D Bi_2O_2Se with controlled thickness for electronics *Small* **19** 2206648
[89] Zhang K, Bao C, Gu Q, Ren X, Zhang H, Deng K, Wu Y, Li Y, Feng J and Zhou S 2016 Raman signatures of inversion symmetry breaking and structural phase transition in type-II Weyl semimetal $MoTe_2$ *Nat. Commun.* **7** 13552
[90] Cheon Y, Lim S Y, Kim K and Cheong H 2021 Structural phase transition and interlayer coupling in few-layer 1T′ and Td $MoTe_2$ *ACS Nano* **15** 2962–70
[91] Paul S, Karak S, Mandal M, Ram A, Marik S, Singh R P and Saha S 2020 Tailoring the phase transition and electron-phonon coupling in 1T′-$MoTe_2$ by charge doping: a Raman study *Phys. Rev. B* **102** 054103
[92] Kuiri M, Das S, Muthu D V S, Das A and Sood A K 2020 Thickness dependent transition from the 1T′ to Weyl semimetal phase in ultrathin $MoTe_2$: electrical transport, noise and raman studies *Nanoscale* **12** 8371–8
[93] Ryu H *et al* 2021 Anomalous dimensionality-driven phase transition of $MoTe_2$ in Van der Waals heterostructure *Adv. Funct. Mater.* **31** 2107376
[94] Deng J, Liu Y, Li M, Xu S, Lun Y, Lv P, Xia T, Gao P, Wang X and Hong J 2020 Thickness-dependent in-plane polarization and structural phase transition in van der Waals ferroelectric $CuInP_2S_6$ *Small* **16** 1904529
[95] Guan Z *et al* 2022 Electric-field-induced room-temperature antiferroelectric−ferroelectric phase transition in van der Waals layered GeSe *ACS Nano* **16** 1308–17
[96] Keum D H *et al* 2015 Bandgap opening in few-layered monoclinic $MoTe_2$ *Nat. Phys.* **11** 482–6
[97] Cho S *et al* 2015 Phase patterning for ohmic homojunction contact in $MoTe_2$ *Science* **349** 625–8
[98] Lyu F, Li X, Tian J, Li Z, Liu B and Chen Q 2022 Temperature-driven α-β phase transformation and enhanced electronic property of 2H α-In2Se_3 *ACS Appl. Mater. Interfaces* **14** 23637–44
[99] Igo J, Gabel M, Yu Z-G, Yang L and Gu Y 2019 Photodefined in-plane heterostructures in two-dimensional In_2Se_3 nanolayers for ultrathin photodiodes *ACS Appl. Nano Mater.* **2** 6774–82
[100] Li T *et al* 2022 Structural phase transitions between layered indium selenide for integrated photonic memory *Adv. Mater.* **34** 2108261
[101] Song S, Keum D H, Cho S, Perello D, Kim Y and Lee Y H 2016 Room temperature semiconductor−metal transition of $MoTe_2$ thin films engineered by strain *Nano Lett.* **16** 188–93
[102] Zhang F, Zhang H, Krylyuk S, Milligan C A, Zhu Y, Zemlyanov D Y, Bendersky L A, Burton B P, Davydov A V and Appenzeller J 2019 Electric-field induced structural transition in vertical $MoTe_2$- and $Mo_{1-x}W_xTe_2$-based resistive memories *Nat. Mater.* **18** 55–61
[103] Li Y, Duerloo K-A N, Wauson K and Reed E J 2016 Structural semiconductor-to-semimetal phase transition in two-dimensional materials induced by electrostatic gating *Nat. Commun.* **7** 10671
[104] Zhu X, Li D, Liang X and Lu W D 2019 Ionic modulation and ionic coupling effects in MoS_2 devices for neuromorphic computing *Nat. Mater.* **18** 141–8
[105] Ciarrocchi A, Tagarelli F, Avsar A and Kis A 2022 Excitonic devices with van der Waals heterostructures: valleytronics meets twistronics *Nat. Rev. Mater.* **7** 449–64
[106] Woods C R, Ares P, Nevison-Andrews H, Holwill M J, Fabregas R, Guinea F, Geim A K, Novoselov K S, Walet N R and Fumagalli L 2021 Charge-polarized interfacial superlattices in marginally twisted hexagonal boron nitride *Nat. Commun.* **12** 347
[107] Kim D S *et al* 2024 Electrostatic moiré potential from twisted hexagonal boron nitride layers *Nat. Mater.* **23** 65–70
[108] Kazmierczak N P, Van Winkle M, Ophus C, Bustillo K C, Carr S, Brown H G, Ciston J, Taniguchi T, Watanabe K and

Bediako D K 2021 Strain fields in twisted bilayer graphene *Nat. Mater.* **20** 956–63
[109] Ko K *et al* 2023 Operando electron microscopy investigation of polar domain dynamics in twisted van der Waals homobilayers *Nat. Mater.* **22** 992–8
[110] Wang Y-H *et al* 2021 *In situ* Raman spectroscopy reveals the structure and dissociation of interfacial water *Nature* **600** 81–85
[111] Chen J, Hu C-L, Kong F and Mao J-G 2021 High-performance second-harmonic-generation (SHG) materials: new developments and new strategies *Acc. Chem. Res.* **54** 2775–83
[112] Cui C, Xue F, Hu W J and Li L-J 2018 Two-dimensional materials with piezoelectric and ferroelectric functionalities *npj 2D Mater. Appl.* **2** 18
[113] Wilkinson A J and Hirsch P B 1997 Electron diffraction based techniques in scanning electron microscopy of bulk materials *Micron* **28** 279–308
[114] Song W, Fei R and Yang L 2017 Off-plane polarization ordering in metal chalcogen diphosphates from bulk to monolayer *Phys. Rev. B* **96** 235420
[115] Dziaugys A *et al* 2020 Piezoelectric domain walls in van der Waals antiferroelectric $CuInP_2Se_6$ *Nat. Commun.* **11** 3623
[116] Zheng C *et al* 2018 Room temperature in-plane ferroelectricity in van der Waals In_2Se_3 *Sci. Adv.* **4** eaar7720
[117] Xu C *et al* 2020 Two-dimensional antiferroelectricity in nanostripe-ordered In_2Se_3 *Phys. Rev. Lett.* **125** 047601
[118] Xu C *et al* 2021 Two-Dimensional Ferroelasticity in van Der Waals β′-In_2Se_3 *Nat. Commun.* **12** 3665
[119] Jeong J *et al* 2022 Ferroelastic–ferroelectric multiferroicity in van der Waals Rhenium dichalcogenides *Adv. Mater.* **34** 2108777
[120] Du R, Wang Y, Cheng M, Wang P, Li H, Feng W, Song L, Shi J and He J 2022 Two-dimensional multiferroic material of metallic p-doped SnSe *Nat. Commun.* **13** 6130
[121] Yasuda K 2023 Electric switch found for a superconductor *Nature* **613** 33–34
[122] Xiao J *et al* 2020 Berry curvature memory through electrically driven stacking transitions *Nat. Phys.* **16** 1028–34
[123] Burch K S, Mandrus D and Park J G 2018 Magnetism in two-dimensional van der Waals materials *Nature* **563** 47–52
[124] Kurebayashi H, Garcia J H, Khan S, Sinova J and Roche S 2022 Magnetism, symmetry and spin transport in van der Waals layered systems *Nat. Rev. Phys.* **4** 150–66
[125] Liu X, Pyatakov A P and Ren W 2020 Magnetoelectric coupling in multiferroic bilayer VS_2 *Phys. Rev. Lett.* **125** 247601
[126] Xu C, Chen P, Tan H, Yang Y, Xiang H and Bellaiche L 2020 Electric-field switching of magnetic topological charge in type-I multiferroics *Phys. Rev. Lett.* **125** 037203
[127] Nataf G F, Guennou M, Gregg J M, Meier D, Hlinka J, Salje E K H and Kreisel J 2020 Domain-wall engineering and topological defects in ferroelectric and ferroelastic materials *Nat. Rev. Phys.* **2** 634–48
[128] Nelson C T *et al* 2011 Domain dynamics during ferroelectric switching *Science* **334** 968–71
[129] Gao P, Britson J, Jokisaari J, Nelson C T, Baek S-H, Wang Y, Eom C-B, Chen L-Q and Pan X 2013 Atomic-scale mechanisms of ferroelastic domain-wall-mediated ferroelectric switching *Nat. Commun.* **4** 2791
[130] Kalinin S V *et al* 2022 Machine learning in scanning transmission electron microscopy *Nat. Rev. Meth. Primers* **2** 11
[131] Son J, Kim K-H, Ahn Y H, Lee H-W and Lee J 2019 Strain engineering of the Berry curvature dipole and valley magnetization in monolayer MoS_2 *Phys. Rev. Lett.* **123** 036806
[132] Yokota H, Matsumoto S, Hasegawa N, Salje E and Uesu Y 2020 Enhancement of polar nature of domain boundaries in ferroelastic $Pb_3(PO_4)_2$ by doping divalent-metal ions *J. Phys.: Condens. Matter* **32** 345401
[133] Lin Y-C, Dumcenco D O, Huang Y-S and Suenaga K 2014 Atomic mechanism of the semiconductingto-metallic phase transition in single-layered MoS_2 *Nat. Nanotechnol.* **9** 391–6
[134] Martin L and Rappe A 2017 Thin-film ferroelectric materials and their applications *Nat. Rev. Mater.* **2** 16087
[135] Zhu J *et al* 2023 Low-thermal-budget synthesis of monolayer molybdenum disulfide for silicon back-end-of-line integration on a 200 mm platform *Nat. Nanotechnol.* **18** 456–63
[136] Yang H, Pan L, Xiao M, Fang J, Cui Y and Wei Z 2020 Iron-doping induced multiferroic in two-dimensional In_2Se_3 *Sci. China Mater.* **63** 421–8
[137] Cheema S S *et al* 2020 Enhanced ferroelectricity in ultrathin films grown directly on silicon *Nature* **580** 478–82
[138] Noheda B, Nukala P and Acuautla M 2023 Lessons from hafnium dioxide-based ferroelectrics *Nat. Mater.* **22** 562–9
[139] Spaldin N A and Ramesh R 2019 Advances in magnetoelectric multiferroics *Nat. Mater.* **18** 203–12
[140] Xia Q and Joshua Yang J 2019 Memristive crossbar arrays for brain-inspired computing *Nat. Mater.* **18** 309–23
[141] Hou W *et al* 2024 Strain engineering of vertical molybdenum ditelluride phase-change memristors *Nat. Electron.* **7** 8–16
[142] Sarwat S G, Kersting B, Moraitis T, Jonnalagadda V P and Sebastian A 2022 Phase-change memtransistive synapses for mixed-plasticity neural computations *Nat. Nanotechnol.* **17** 507–13
[143] Liu B L and Cheng H-M 2023 2D ferroelectricity in hetero-phase junction *Nat. Nanotechnol.* **18** 5–6
[144] Pacchioni G 2023 One material, three phases *Nat. Rev. Mater.* **8** 7
[145] Lipatov A *et al* 2022 Direct observation of ferroelectricity in two-dimensional MoS_2 *npj 2D Mater. Appl.* **6** 18
[146] Li L *et al* 2019 Emerging in-plane anisotropic two-dimensional materials *InfoMat* **1** 54–73